HHS Public Access

Author manuscript

Biomed Pharmacother. Author manuscript; available in PMC 2024 March 01.

Published in final edited form as:

Biomed Pharmacother. 2023 March ; 159: 114255. doi:10.1016/j.biopha.2023.114255.

Identification and characterization of a first-generation inhibitor of claudin-1 in Colon Cancer progression and metastasis

Iram Fatima[1], **Jaya Prakash Uppada**[1], **Yashpal S. Chhonker**[2], **Saiprasad Gowrikumar**[1], **Susmita Barman**[1], **Sourav Roy**[3], **Kirsten T. Tolentino**[4], **Nicholas Palermo**[5], **Amar Natarajan**[6], **Daniel R Beauchamp**[7], **Alex Vecchio**[3], **Daryl J. Murry**[2,8], **Amar B. Singh**[1,8,9], **Corey R. Hopkins**[4], **Punita Dhawan**[1,8,9]

[1]Department of Biochemistry and Molecular Biology, University of Nebraska Medical Center, Omaha, NE, USA

[2]Department of Pharmacy Practice and Science, University of Nebraska Medical Center, Omaha, NE, USA

[3]Department of Biochemistry, University of Nebraska-Lincoln, Lincoln, Nebraska 68588-0664, United States, University of Nebraska Medical Center, Omaha, NE, USA

[4]Department of Pharmaceutical Sciences, University of Nebraska Medical Center, Omaha, NE, USA

[5]Computational Chemistry Core, University of Nebraska Medical Center, Omaha, NE, USA

[6]Eppley Institute for Cancer Research, University of Nebraska Medical Center, Omaha, NE, USA

[7]Surgical Oncology Research Laboratories, Department of Surgery, Vanderbilt University Medical Center, Nashville, Tennessee, USA, University of Nebraska Medical Center, Omaha, NE, USA

[8]VA Nebraska-Western Iowa Health Care System, Omaha, NE, University of Nebraska Medical Center, Omaha, NE, USA

[9]Buffet Cancer Center, University of Nebraska Medical Center, Omaha, NE, USA

Abstract

Colorectal cancer (CRC) is a leading cause of the cancer-related deaths worldwide. Thus, developing novel and targeted therapies for inhibiting CRC progression and metastasis is urgent. Several studies, including ours, have reported a causal role for an upregulated claudin-1 expression in promoting CRC metastasis through the activation of the Src and β-catenin-signaling. In murine models of colon tumorigenesis, claudin-1 overexpression promotes oncogenic properties such as transformation and invasiveness. Conversely, the downregulation of claudin-1 inhibits colon tumorigenesis. Despite being a desirable target for cancer treatment, there are currently no known claudin-1 inhibitors with antitumor efficacy. Using a rigorous analytical design and implementing *in- vitro* and *in-vivo* testing and a brief medicinal chemistry campaign, we identified a claudin-1-

To whom correspondence should be addressed: Punita Dhawan, Ph. D, Departments of Biochemistry and Molecular Biology, University of Nebraska Medical Center, Omaha, NE-68022, USA, Tel: (402)-559-6587; Fax: (402)-559-6650, punita.dhawan@unmc.edu.

Conflict Of Interest: None to declare.

specific inhibitor and named it I-6. Despite its high potency, I-6 was rapidly cleared in human liver microsomes. We, therefore, synthesized I-6 analogs and discovered a novel small molecule, PDS-0330. We determined that PDS0330 inhibits claudin-1-dependent CRC progression without exhibiting toxicity in *in-vitro* and *in-vivo* models of CRC and that it binds directly and specifically to claudin-1 with micromolar affinity. Further analyses revealed that PDS-0330 exhibits antitumor and chemosensitizer activities with favorable pharmacokinetic properties by inhibiting the association with metastatic oncogene Src. Overall, our data propose that PDS-0330 interferes with claudin-1/Src association to inhibit CRC progression and metastasis. Our findings are of direct clinical relevance and may open new therapeutic opportunities in colon cancer treatment and/or management by targeting claudin-1.

Keywords

Claudin-1; Colon Cancer; Src; chemoresistance

1. Introduction:

Colorectal cancer (CRC) is the third most common malignant cancer worldwide, with the second highest mortality rate. According to the American Cancer Society, CRC diagnoses in United States are expected to reach 1.9 million in 2022 [1, 2]. Despite recent breakthroughs in detection and treatment, the 5-year survival rate for stage-IV CRC patients is still a dismal 12% and has been stable for a long time [3]. Unfortunately, over two-thirds of newly diagnosed CRC patients have metastases at the time of diagnosis. Currently, there are no effective ways to prevent or delay CRC metastasis, and minimal therapeutic options available that include surgery, which is combined with radiotherapy, chemotherapy, targeted therapy, and other treatments [4, 5]. However, due to the intricate mechanism of CRC occurrence, development, and metastasis, specific targeted drugs for CRC treatment are still lacking. Thus, for effective clinical management of malignant CRC and to overcome the limitations of standard chemotherapy, the development of novel drugs is urgent.

Several investigations, including ours have now validated that upregulated claudin-1 expression plays a causal role in promoting CRC progression and metastasis [6]. Claudins are membrane proteins that govern the barrier properties of tight junctions [7, 8] and are being investigated as possible therapeutic targets for antibody/inhibitor-based treatments [9]. They are composed of four transmembrane domains, two extracellular loops, and cytoplasmic tails [10, 11]. Claudin-1 is one of 27 claudin family members [12]. Claudin-1 has been found to be overexpressed in primary CRC and metastasis, as well as in CRC cell lines [6, 13–15], with notable changes in its location. Claudin-1 overexpression in tumor cells can cause changes in tight junction structure and function, as well as dysregulation of cell signaling pathways [16]. Claudin-1 has also been shown to play a role in Wnt and Notch signaling which contribute to cancer progression and metastasis [17, 18]. Further, we demonstrated the role of claudin-1 in resistance to anoikis [19]. Anoikis, a type of apoptosis that occurs when cells separate from the extracellular matrix, is an important mechanism in tissue homeostasis, development, and metastasis [20]. Claudin-1 controlled cell anoikis in colon cancer by regulating E-cadherin/β-catenin/Tcf and Src signaling [6, 17,

19, 21]. Overall, it appears that claudin-1 plays a major role in colon cancer progression and metastasis. Much effort has been focused on understanding claudin-1 function and regulation in cancer; however, little is known about its potential utility as a therapeutic target. So far, no known small molecule inhibitors for claudin-1 exist that can inhibit claudin-1-dependent oncological functions. The aim of this study is to address this critical clinical need and focus on development and preclinical testing of a novel small molecule inhibitor of claudin-1, with the high promise of curbing CRC progression, metastasis as well as chemoresistance.

We used a rigorous analytical design that encompassed *in-vitro* and *in-vivo* analyses to discover a claudin-1-selective inhibitor I-6. I-6 exhibited high potency. However, due to its rapid metabolism and thus limited efficacy, several small molecule analogs were synthesized. Screening of I-6 analogsand subsequent characterization showed that PDS-0330 was a unique and selective inhibitor of claudin-1-dependent CRC progression that was metabolically stable and had favorable pharmacokinetic properties. The originality of this inhibitor resides not only in its discovery but also in its mechanism of action, as we show that its effects are limited to colon cancer cells while normal cells are not affected. Overall, our findings suggest that PDS-0330 may prevent CRC progression and metastasis by interfering with claudin-1 binding to Src. This then results in inhibition of the resistance to anoikis, invasion and tumorigenic potential in claudin-1 overexpressed cells. These results have clear clinical implications and could lead to novel therapeutic opportunities in colon cancer treatment and/or management.

2.0. Materials and Methods:

2.1. Compound and reagents

Antibodies against claudin-1 (# 71–7800) and claudin-4 (# 36–4800) were purchased from Thermo Fischer Scientific (Waltham, MA USA). The anti-PARP (#5625S), anti-Bcl2 (#15071S), anti-Bcl-xL (#2764S), anti-Ki67 (#12202S), anti-survivin (# 2808S), anti-Src (#2123S), anti-p- Src (Tyr416) (#6943S), anti-pAkt (#4060S) and anti-Akt (#9272S) antibodies were purchased from Cell Signaling Technology, Inc. (Danvers, MA, USA). The anti-GAPDH antibody was from Proteintech (#60004–1-Ig) (Rosemont, IL, USA). The anti-β-Actin antibody (# sc-47778) was purchased Santa Cruz Biotechnology, Inc. (Dallas, Texas, USA). 5-fluorouracil (5-FU) was procured from the University of Nebraska Medical Center (UNMC), Omaha, USA pharmacy. Blood Urea Nitrogen (BUN) (# EIABUN) and Aspartate aminotransferase (#701640) colorimetric assay kits were purchased from Thermo Fischer Scientific (Waltham, MA USA) and Cayman Chemical (Ann Arbor, Michigan 48108 USA) respectively.

2.2. Chemical Synthesis of I-6 and PDS-0330-

To a mixture of **1** or **2** (1.9 mmol) in CH3CN (5 ml) was treated with SOCl2 (0.18 ml), and the resulting mixture was refluxed for 2 h. The solvent was removed *in vacuo* to provide the crude product (**3** or **4**) as an oil which was used in the next step without further purification. To the corresponding SM (**3** or **4**) (0.45 mmol) was added over 5 min to a freshly prepared solution of (0.49 mmol) NH4SCN in 4 ml acetone, and the mixture was heated to reflux

for 15 min. The *in situ* generated benzoyl isothyocyanate was reacted with (0.45 mmol) of respective amine (4- (benzo[*d*]oxazol-2-yl) aniline for **3** and 4-(1*H*-benzo[*d*]imidazol-2-yl)aniline for **4**) in 4 ml acetone. The mixture was heated to reflux for 30 min, and then poured on ice with vigorous stirring. The resulting solid was collected and washed with H2O, followed by cold acetone, and dried over a vacuum.

N-((4-(benzo[*d*]oxazol-2-yl)phenyl)carbamothioyl)-2-naphthamide (**5, KVA-E-23A, PDS-0330).** Yield = 120.5 mg; 54% yield, off-white solid. LCMS: RT = 3.424 min., ESI-MS: *m/z* $[M + H]^+$, calc'd 424.11 for $C_{25}H_{18}N_3O_2S$, found 424.00. ^{1}H NMR (499 MHz, DMSO-*d*6) δ 12.90 (s, 1H), 11.86 (s, 1H), 8.75 (d, *J* = 1.9 Hz, 1H), 8.27 (d, *J* = 8.3 Hz, 2H), 8.22 – 7.94 (m, 6H), 7.82 (ddd, *J* = 9.5, 6.9, 2.4 Hz, 2H), 7.69 (dt, *J* = 22.6, 7.1 Hz, 2H), 7.44 (tt, *J* = 7.8, 5.9 Hz, 2H). ^{13}C NMR (126 MHz, DMSO) δ 179.43, 162.30, 150.72, 142.04, 141.66, 135.42, 132.20, 130.62, 129.89, 129.22, 128.64, 128.30, 127.57, 126.01, 125.41, 124.78, 124.21, 120.28, 111.41.

N-((4-(1*H*-benzo[*d*]imidazol-2-yl)phenyl)carbamothioyl)-3-methoxy-2-naphthamide (**5, I-6, KVA-E-25B)**. Yield = 10.5 mg; 7% yield, off-white solid. LCMS: RT = 2.936 min, ESI-MS: *m/z* $[M + H]^+$, calc'd 453.14 for $C_{26}H_{21}N_4O_2S$, found 451.11. ^{1}H NMR (499 MHz, DMSO-d_6) δ 12.96 (s, 1H), 12.78 (s, 1H), 11.57 (s, 1H), 8.50 (s, 1H), 8.29 – 8.21 (m, 2H), 8.06 (d, *J* = 8.1 Hz, 1H), 7.96 (dd, *J* = 19.3, 8.4 Hz, 3H), 7.71 – 7.55 (m, 2H), 7.48 (ddd, *J* = 8.1, 6.8, 1.2 Hz, 1H), 7.30 –7.18 (m, 2H), 4.09 (s, 3H). ^{13}C NMR (126 MHz, DMSO) δ 166.47, 154.38, 151.12, 136.51, 132.84, 129.42, 127.90, 127.30, 127.07, 125.33, 124.72, 122.58, 120.17, 119.44, 119.20, 116.73, 107.89, 56.99 (Suppl Fig 1A).

2.3. Cell culture and transfection

The human colon cancer cell lines HCT116, SW480, and SW620 and normal epithelium IEC-6 cells were obtained from ATCC and cultured in RPMI containing 10% FBS. The generation and culture conditions for the $SW480^{control}$, $SW480^{cld1}$ (claudin-1 overexpressing), $SW480^{cld2}$ (claudin- 2 overexpressed), $SW620^{control}$, and $SW620^{1C}$ (claudin-1 knockdown) cells, used in current studies, have been described previously [6]. Cell proliferation was measured using PrestoBlue Cell Viability Reagent (Invitrogen # A13262), according to the manufacturer's protocol. Cells were transfected using Turbo DNAfectinTM 3000 reagents (#TDNAF-1000 MidSci), according to the manufacturer's protocol.

2.4. Anoikis-induced apoptosis

Anoikis was induced by plating cells on poly-HEMA-coated culture plates, and apoptosis was determined using the Cell Death Detection $ELISA^{PLUS}$ kit (Roche Diagnostics Corp.) as described previously [6].

2.5. Immunohistochemistry analysis

These analyses were performed using the standard protocols as described before [22]. Anti-Ki67 and anti-cleaved PARP antibodies were used for IHC.

2.6. Cell extraction and Western blotting

Treated cells were lysed as previously described [23]. 10–30μg of protein were loaded per lane and separated by sodium dodecyl sulfate-polyacrylamide gel electrophoresis (SDS-PAGE) 8% or 10% or 12% gels. After transfer, Immobilon-P (Millipore) was immunoblotted using the primary antibodies. Conjugated secondary antibodies (#HAF007 anti-Mouse, #HAF008 anti-Rabbit, R&D Systems, Minneapolis, MN) were used according to the manufacturer's protocols. Protein bands were observed on X-ray film (Classic blue autoradiography film BX) using an enhanced chemiluminescence detection system (#50–904-9326, Perkin Elmer).

2.7. Soft Agar Assay

Anchorage-independence growth assay or soft agar assay was used to determine the growth potential of control and treated cells as previously described [22]. Each group was plated in triplicates. After three weeks, viable colony numbers and sizes were counted and measured.

2.8. Transwell migration assay

An invasion assay was carried out using 24-well plate (#07–200-169, Corning). A polyvinyl-pyrrolidone-free polycarbonate filter (8 μm pore size) was coated with matrigel (#356237, Corning). Briefly, transfected cells were trypsinized and seeded onto the upper chambers of the trans-well (0.5×10^5 cells/well) coated with matrigel in a serum-free medium. The lower chambers of the trans-well were filled with RPMI medium containing 10% FBS. After incubating at 37°C and 5% CO2 for 48 h, cells on the upper surface of the filter were removed using a cotton swab, whereas cells invasive through the filter to the lower surface were fixed with 4% paraformaldehyde for 10 min and stained with 0.1% crystal violet for 20 min. Cells were observed and counted at five random fields using a light microscope (Olympus).

2.9. Tumoroid Culture

The tumor from the $APC^{min/+}$/ claudin-1 transgenic mice was isolated and cultured in-vitro as per the previous protocol [24]. Briefly, the adenomas were isolated and washed with ice-cold PBS. The adenomas were incubated in EDTA chelation buffer to remove the loose epithelium and retain the tumor mass. Further washing of the tumors with ice-cold PBS was carried out. The tumors were fragmented with a digestion buffer containing collagenase. The single-cell tumor suspension was further washed by centrifugation at 200 x g for 3 min. The pelleted tumor cells were resuspended in Matrigel (Corning) and plated in 24 well plates for further experiment.

2.10. Xenograft-tumor studies

All animal experiments were conducted with the approval of the Institutional Animal Care and Use Committee (IACUC) of UNMC. The tumorigenicity of cells under study was assessed using subcutaneous flank inoculation of 1×10^6 cells or PDX tumor chunk (~$2mm^3$) in 6-week-old athymic nude mice. Animals were assessed for 4–9 weeks after the inoculation for tumor incidence and growth and then were sacrificed. Tumor volume was

measured using the formula tumor volume = 1/2(length × width^2)/2 as previously described [25].

2.11. Blood Urea Nitrogen (BUN) and Aspartate aminotransferase colorimetric assay

BUN levels in plasma and renal tissue lysate were determined according to the manufacturer's instructions for kidney function analysis (# EIABUN). Aspartate aminotransferase activity was tested in plasma and liver tissue according to the manufacturer's instructions (#701640) to assess the effect of inhibitors on liver function.

2.12. MST (Microscale thermophoresis) measurement

Human claudin-1 and other orthologs with a decahistidine tag and thrombin protease site at their N-termini were expressed and purified according to previously reported protocols [26]. Cy3 labeling with 50 μg mono-NHS-Cy3 per 1 mg claudin occurred on-column using immobilized metal affinity chromatography (IMAC) and consisted of Cy3 being added to claudins in a buffer containing 50 mM HEPES, pH 7.4/8.0, 150 mM NaCl, 5% glycerol, and 0.04% n-Dodecyl-β-D- Maltopyranoside (DDM). The dye was mixed well with claudins and incubated for 4 hours at 4°C. Post-labeled claudins were washed using 20 column volumes in a buffer containing 50 mM TRIS, pH 7.4, 300 mM NaCl, 5% glycerol, 40 mM imidazole, and 0.04% DDM to quench the reaction and remove the free dye. Cy3-labeled claudins were released from the IMAC resin with thrombin digestion at 4°C overnight in a buffer containing 50 mM TRIS, pH 8.0, 150 mM NaCl, 5% glycerol, and 0.04% DDM. Purified protein post-IMAC was ~90% pure as assessed by SDS- PAGE. Further polishing was performed using size-exclusion chromatography (SEC), where the final protein was eluted in MST Assay buffer containing 10 mM HEPES, pH 7.4, 100 mM NaCl, 4% glycerol, and 0.04% DDM and used for binding studies. Trypsin digestion of claudin-1 was performed by incubating post-IMAC pure claudin-1 and trypsin immobilized on agarose beads (ProteoChem) together at a 50:1 molar ratio (claudin: trypsin) overnight at 4°C. The following day the trypsin beads were captured, and Cy3-labeled and trypsinized claudin-1 was subjected to SEC and then used for binding studies.

MST measurements were performed using a Monolith instrument (NanoTemper Technologies). Powdered PDS-0330 was dissolved in dimethyl sulfoxide (DMSO) to a concentration of 135 μM, which was necessary due to limited solubility in aqueous buffers. The concentration of PDS-0330 for analyses were varied from 4 nM to 135 μM, while the concentrations of Cy3-claudins were fixed at 1 μM. The PDS-0330 sub-dilutions were mixed with Cy3-claudins and loaded in standard monolith NT.115 capillary tubes for measurements. Experiments were conducted at 25° or 37°C using the nano-green channel of the Monolith instrument, and the data comprising 2–8 individual experiments were analyzed using GraphPad Prism, version 9 (GraphPad Software, San Diego, California).

2.13. Pharmacokinetics (PK) and bio-distribution studies

The University of Nebraska Medical Center Institutional Animal Ethics Committee approved all animal studies (protocol number 17–046-06-FC). Male and Female BALB/c or black 6 mice, with weights ranging from 24 to 30 grams, were used for PK and bio-distribution studies. Animals were housed in the University of Nebraska Medical Center

animal facility for at least seven days prior to the experiments, in order to acclimatize the animals to the laboratory conditions, at a temperature of 23–24 ○C, relative humidity of 40–70%, and 12/12 h light/dark cycles. The dosing solution was made of DMSO-Polyethylene glycol 400 (PEG400)-Propylene glycol (PG)-EtOH-Cremophore- PBS (2/20/10/10/5/53 % v/v). I-6 was administered by oral gavage (5mg/kg) and intravenous (1mg/kg) via the tail vein. PDS-0330 was administered by oral gavage (5mg/kg) and intraperitoneal (IP) (5mg/kg). The dose was selected based on previous pharmacological efficacy experiments in mice. After dosing, approximately 100 μl of blood was collected in a polypropylene tube from the maxillary vein at 5, 15, 30 minutes, and 1, 2, 4, 6, 8, and 24 h. Two blood time points were collected from every mouse, and the third time point was the terminal time point, for a total of three-time points from each mouse (5 mice/ group/ per time point). Plasma was prepared by centrifugation at 4,000 x g at 4 °C for 10 minutes. The collected plasma samples were stored at −80 °C until analysis.

Tissues (liver, lungs, heart, kidney, brain, and spleen) were collected at 2, 8- and 24 h following dosing. Tissue samples were rinsed with phosphate-buffered saline to remove the blood and then blotted with filter paper. After weighing, each tissue sample was individually homogenized with de-ionized water, 5-dilution factor for the liver, spleen, brain, lungs, and kidney, while the heart was homogenized at a 6-dilution factor using a TissueLyser II (Qiagen Science, KY), then all tissues were stored at −80 ℃ until analysis. Plasma concentrations (ng/ml) and tissue concentrations (ng/g) were determined for each time point collected. Drug accumulation in tissue was determined by calculating a tissue to plasma concentration ratio (t:p) for each tissue.

All plasma and tissue samples were analyzed via a validated LC-MS/MS method with a lower limit of quantitation of 0.1 ng/ml for both compounds. The MS/MS system was operated at unit resolution in the multiple reaction monitoring (MRM) mode, using precursor ion → product ion combinations of 453.05→252.2 m/z and 424.10>253.05 for I-6 and PDS-0330, respectively. Plasma and tissue samples (50 μl) were processed by simple protein precipitation. All samples were quenched with 300 μl of acetonitrile spiked with 10 μl of internal standard (IS; 0.5 μg/ml), then vortexed and centrifuged at 13,000 x g for 15 min. The supernatant was collected, transferred to an autosampler vial, and injected (2 μl) onto the LC-MS/MS system.

The PK parameters of I-6 and PDS-0330 in plasma and tissues were calculated using non-compartmental analysis with Phoenix WinNonlin 8.3 (Certara, Princeton, NJ). The area under the curve ($AUC^{0-\infty}$) was estimated using the linear trapezoidal method from 0-tlast and extrapolation from tlast to infinity based on the observed concentration at the last time point divided by the terminal elimination rate constant (k_e). The elimination half-life ($t_{1/2}$) was calculated using the equation 0.693/k. Clearance (Cl/F) and the volume of distribution of the elimination phase (Vd/F) were calculated as dose/$AUC_{0-\infty}$ and dose/k*$AUC_{0-\infty}$, respectively. Mean tissue concentrations were calculated and expressed as ng/g tissue. Drug accumulation in tissue was determined by calculating a tissue to plasma concentration ratio (t:p) for each tissue.

2.14. Metabolic stability assay:

Metabolic stability for I-6 and PDS-0330 was assessed using human liver microsomes (HLM) (XenoTech, LLC, Lenexa, KS, USA) for phase I metabolism. Briefly, the buffer solution was prepared containing potassium phosphate buffer (100 mM, pH 7.4), 25 µl of microsomal protein (20 mg/ml), magnesium chloride (10 mM), and NADPH (2 mM) in a final volume of 0.5 ml was pre-incubated at 37 °C for 10 min in water bath maintaining at 60 rpm. The reaction was started by adding 2µl of I-6 or PDS-0330 (1 µg/ml). Serial samples (50 µl) were collected at selected time intervals (0, 5, 15, 20, 30, 45, and 60 minutes) and quenched with 300 µl of acetonitrile spiked with 10 µl of IS (0.5 µg/ml).

In-vitro phase I and II metabolism were assessed using mouse liver S9 fractions (XenoTech, LLC, Lenexa, KS, USA). Briefly, 1 µg/ml, I-6 was pre-mixed with a solution mixture of potassium phosphate buffer (100 mM, pH 7.4) at 37 °C containing the following: 1 mM NADPH, 4 mM saccharolactone, 1 mM uridine 4′-diphospho-glucuronic acid, and 0.1 mM 3′-phosphoadenosin- 4′-phosphosulphate. Incubation was performed in triplicate, n=3. Immediately after mixing the, I- 6 or PDS-0330 into the incubation mixture, a sampling point was taken, representing t = 0.

Subsequent sampling points were performed at the following intervals: 5, 15, 20, 30, 45, 60, 90, and 120 minutes. To stop the reaction, 50 µl of the sample were added to 1.5 ml-centrifuge tube containing 300 µl of ice-cold ACN spiked with 10 µl of IS (0.5 µg/ml). All samples were vortexed and centrifuged at 13,000 x g for 10 min. The resultant supernatant was transferred to an autosampler vial, and 2 µl was injected into the LC-MS/MS. Testosterone, 7-HC, and diclofenac were utilized as positive controls to ensure proper incubation conditions were maintained.

The HLM and mouse S9 metabolic stability results were expressed as the percentage of drug remaining at each time point. The *in-vitro* metabolic elimination rate constant was calculated from the first-order plot of a natural logarithm of the area ratio versus time. The slope of the linear regression equation was used to determine the elimination rate constant “k” (min-1). The half-life (t1/2) was calculated using equation 9. The *in-vitro* intrinsic clearance (CLint) was determined by using equation 10. The intrinsic clearance was further extrapolated to in vitro hepatic clearance (CLint, H: ml/min/kg of body weight) using a scaling factors and Equation 11 [27, 28].

$$t^{1/2} = 0.693/k$$

$$CL_{int} = \frac{0.693}{t^{1/2}} \times \frac{Volume\ of\ reaction\ mixture\ (ml)}{mg\ of\ protein}$$

$$CL_{int,H} = CL_{int} \times \frac{mg\ of\ protein}{gram\ of\ liver} \times \frac{gram\ of\ liver}{kg\ of\ body\ weight}$$

2.15. Statistical methods:

For all the experiments, statistical analysis was performed using GraphPad Prism version 9 (GraphPad Software). All experiments have been performed in triplicates. Normally distributed data were expressed as the mean ± SD and analyzed using Student's t-test. Multiple comparisons were performed using one-way or two-way ANOVA and the significance level was set at $P < 0.05$. Quantification of IHC analysis and immunoblotting analysis was performed using ImageJ software.

3.0. Results:

3.1. Identification and Validation of claudin-1 Inhibitors *in-silico* and *in-vitro*:

Using YASARA, the primary sequence of human claudin-1 was unfolded, and cavities that can be targeted by small molecules were defined using Molegro Virtual Docker (MVD). MVD is an integrated platform for predicting protein-ligand interactions. MVD is used in the preparation of the molecules to determine the potential binding sites of the target protein and prediction of the binding modes of the ligands. The 100K small molecule library was screened in silico using MVD. The top 10 inhibitors that bound to site 3 (Fig 1 Ai&Aii) with the best binding energies were selected as hits and were used for biological studies. These top 10 inhibitors were further screened by testing their efficacy using the Anoikis assay as detailed below.

Anoikis (apoptosis characterized by a loss of cell-matrix interaction) is a well-established model for predicting cell survival independent of the cell attachment. Anoikis resistance is peculiar to the cancer cells, resulting in cancer growth and metastatic colonization. Claudin-1 expression influences colon cancer invasion and metastasis by modulating anoikis in colon cancer cells [6, 19]. Therefore, the anoikis assay, which plays a crucial role in metastasis, was used to screen these top 10 claudin-1 inhibitors. To determine the effect of these inhibitors' specificity towards claudin-1 expression in relation with anoikis, $SW480^{cld1}$ (stably over-expressing claudin- 1), SW620 (endogenously over-expressed claudin-1), HCT116 (claudin-1 deficient cell line) and/or $SW620^{1C}$ (with shRNA inhibition of claudin-1) cells were used in the study (Suppl Fig 1B). Among the top 10 inhibitors, cells treated with inhibitor-6 (I-6) (Fig1 B) displayed substantial apoptosis/cell death, and inhibition of resistance to anoikis in claudin-1 expressed SW620 and $SW480^{cld1}$ (Fig1 C&D, Suppl Fig1 C, D & Suppl Fig2 A). I-6 had no effect on HCT116 cells or $SW620^{1C}$, implying that I-6 is more specific to claudin-1 expressing cells (Fig1 C&D & Suppl Fig2 A).

The biological activity assays, such as invasion assay, offer a quick and effective evaluation of the therapeutic potential of a lead anti-invasive/anti-metastatic compound (such as I-6). Overexpression of claudin-1 has been linked to metastatic and invasive capabilities of CRC cells [19]. Therefore, we sought to determine if I-6 had any effect on invasion in claudin-1 expressing CRC cells (Fig1 E & Suppl Fig2 B). Invasion was significantly inhibited by 1–6 in claudin-1 high SW620 and $SW480^{cld1}$ cells, however this effect was minimal in HCT116 cells (Fig1 E & Suppl Fig2 B).

Taken together, above findings strongly implied that claudin-1 inhibitors play a key role in the regulation of cellular transformation, and hence could be used to prevent the progression of colon cancer.

3.2. I-6 interferes with tumor formation and enhances the chemosensitivity of colon cancer cells:

Our previous findings showed that claudin-1 overexpression in $SW480^{cld1}$ cells caused tumors to form at a considerably faster rate as compared to $SW480^{control}$ cells [6]. Thus, to determine the therapeutic efficacy of claudin-1 inhibitor I-6 *in-vivo*, we used a xenograft tumor transplantation model with claudin-1 overexpressed SW480 cells. $SW480^{cld1}$ cells were implanted subcutaneously in athymic nude mice. After confirming palpable tumor growth (10 days after initial transplantation), we treated the mice with I-6 (10 mg/kg; once/week) for two weeks (n = 5 mice/group). I-6 administration remarkably decreased tumor volume (mm^3) as early as day 16- days post-transplantation ($p = 0.001$) for $SW480^{cld1}$ cells, and this reduction was maintained throughout the study (Fig 2 Ai&Aii). At the time of necropsy, I-6 -treated tumors volume and weight were significantly reduced compared to the tumors in mice treated with vehicle alone (Fig 2 Aii & Suppl Fig2 C). To validate the tumor inhibiting efficacy of the I-6, the tumors were stained for proliferation marker Ki67 and apoptotic marker cleaved PARP (Fig 2 Aiii & Suppl Fig2 D). Ki67 expression was significantly inhibited by I-6 treatment, whereas cleaved PARP was significantly increased by I-6 treatment (Fig 2 Aiii & Suppl Fig2 D). Overall, this data demonstrated an anti-tumorigenic potential of I-6 in xenografts resulting from claudin-1 overexpressing CRC cells.

Considering the importance of chemoresistance in CRC metastasis [6], we further investigated the adjuvant use of 1–6 with 5-FU. Colon cancer cells were treated with 1–6 alone or in conjunction with 5-FU, a common chemotherapeutic *in-vitro* and *in-vivo*. We observed significantly less % cell survival and thus resistance to anoikis in combination treatments in claudin-1 overexpressing $SW480^{cld1}$ and SW620 cells as compared to either treatment alone (Fig2 B&C). We did observe a significant reduction in the tumor volume in mice receiving combination therapy (I-6 + 5-FU; in $SW480^{cld1}$ xenograft) compared to I-6 or 5-FU alone (Fig2 D). There were no obvious changes in the mouse behavior or weight during these studies. We further confirmed these observations in tumoroids isolated from the $APC^{min/+}$ / Claudin-1 mice. I-6 was tested alone at 25μM and along with the combination of 5-FU (5μM). I-6 administration for 48 hours significantly increased the rate of apoptosis in $APC^{min/+}$ / Claudin- 1 tumoroids, as evidenced by induction of apoptosis (black area) in the representative images (Fig2 E). Significantly higher apoptosis was observed in combination therapy as compared to I-6 or 5-FU alone even at 24 hours (Fig2 E). Overall, our findings suggested that I-6 is a specific claudin-1 inhibitor that might be useful in inhibiting its effects on tumorigenesis and chemoresistance.

3.3. Absorption, distribution, metabolism, and excretion (ADME) pharmacokinetics of I-6 and its metabolic stability

We further determined the *in-vivo* pharmacokinetics parameters of I-6. Following a single intravenous dose of I-6 (1 mg/kg) in mice (C57BL6; n=5), serial blood samples were

obtained, and plasma samples were quantitated for I-6. The plasma concentration vs. time profile after intravenous administration of I-6 in mice is shown in Figure 3Ai. Following the intravenous administration of I-6 mean non-compartmental pharmacokinetic parameters are shown in Table 1.

Following intravenous administration, a peak I-6 concentration of 798 ng/ml was achieved, with an $AUC_{0-\infty}$ o f 1142 hr*ng/ml. I-6 was detectable up to 24 h, with an elimination $t_{,1/2}$= 7.0 h, and clearance and volume of distribution of 0.8 L/h/kg and 8.4 L/kg, respectively (Table 1). In addition, tissue distribution of I-6 was evaluated at 2, 8 and 24 hours. Measurable concentrations of I-6 were detected in all the tissues examined with higher concentrations in the lung and liver tissue (principal sites for CRC metastasis) (Fig 3 Aii). The tissue to plasma concentration ratio (t:p) was greater than 1 for all tissues evaluated except brain. Following the post oral administration of I-6 (5mg/kg) to mice, plasma peak concentrations (Cmax) was 2.8 ng/ml at 2 h (Fig 3 Bi). Oral bioavailability was determined to be <1.0% for I-6. Following oral administration, I-6 concentrations were highest in the liver, with concentrations of 65 ng/gm tissue at 24 hours (Fig 3 Bii).

Metabolic stability studies of I-6 were evaluated using human liver microsomes (HLM) for the *in- vitro* assessment of phase-I metabolism. I-6 was found to be rapidly degraded, with only 49% of the drug remaining after 60 min (Fig4 A). Primary metabolites identified induced acetylation and hydroxylation with glucuronidation (data not shown). Results of *in-vitro* and *in-vivo* PK and drug metabolism studies provided a rationale for the development of 1–6 analogs in order to improve metabolic stability.

3.4. I-6 analog PDS-0330 is more stable and showed better efficacy in claudin-1 overexpressed cells

In order to progress the molecule into advanced *in-vitro* and *in-vivo* studies, a more stable and potent compound was needed. To this end, we synthesized more analogs of I-6 (Suppl Fig3). Among all, PDS-0330, which lacks methoxy and has the benzimidazole group substituted for a benzoxazole, was found to be the most potent in inducing cell death (Suppl Fig3). Besides that, incubations of PDS-0330 with HLM revealed that the compound was more metabolically stable over 60 minutes (90% of PDS-0330 as compared to 49% of I-6 remaining), possibly due to the removal of the methoxy group (Fig4 A). Furthermore, our findings indicated that the PDS-0330 compound's activity was three times higher than that of I-6. PDS-0330 had an EC_{50} of 8.4 μM in $SW480^{cld1}$ cells, whereas I-6 had an EC_{50} of 28.40 μM (Fig 4 Bi). Similarly, in SW620 cells, PDS- 0330 had an EC_{50} of 9.30μM, whereas I-6 had an EC50 of 24.76 μM (Fig 4 Bii). Most importantly, PDS-0330 had no effect on cell growth/survival in claudin-1 deficient HCT116 cells (Fig 4 Biii) or normal IEC-6 cells (Fig 4 Biv).

Given the significance of inhibition of anoikis/apoptosis in the regulation of claudin-1 mediated colon tumorigenesis, we investigated the effect of inhibition using PDS-0330 in claudin-1 overexpressing SW620, $SW480^{cld1}$, claudin-1 deficient HCT116, and claudin-1 inhibited $SW620^{1C}$ cells. In $SW480^{cld1}$ and SW620 cells, PDS-0330 dramatically reduced the resistance to anoikis as % cell death was significantly higher in the treated cells. However, PD-0330 exhibited no effect on HCT116 and $SW620^{1C}$ cells that lacked

claudin-1. Another analog with no impact on claudin-1 mediated cell survival 20A was used as a negative control. (Fig4 C & Suppl Fig4 A).

3.5. PDS-0330 exhibits favorable absorption, distribution, metabolism and excretion (ADME) and Pharmacokinetics

PDS-0330 had good metabolic stability *in-vitro* (Figure 4A). Encouraged by this result and to further gain insights into the preclinical pharmacokinetics and tissue distribution, we subsequently performed analysis following a single intraperitoneal (IP) dose of PDS-0330 (5 mg/kg) and oral dose (5 mg/kg) in mice. The plasma concentration vs. time profile for PDS-0330 is shown in Figure 5A.

Pharmacokinetic data were processed with Phoenix® 8.3 software. The mean non-compartmental pharmacokinetic parameters are shown in Table 2. Following oral and IP administration, PDS- 0330 Cmax was 30.8 ± 18.3 and 59.3 ± 13.8 ng/ml, respectively, with a longer half-life and moderate clearance rate. To assess the distribution of PDS-0330 into tissues, mice were sacrificed at 2, 8, and 24 hours after the PO and IP administration of the drug. Measurable concentrations of PDS- 0330 were detected in all studied tissues (liver and lungs) at 2, 8, and 24 h. The tissue concentrations are shown in Figure 5B and Table 3. PDS-0330 accumulated in all tissues, with higher concentrations in the lung and liver tissue. In addition, our data show that the tissue to plasma concentration ratio (t:p) is ≥1 for the liver and lungs. There was no change in mouse behavior or weight 24 hours after a single PO and IP injection of PDS-0330 (data not shown). The metabolic stability of PDS-0330 studies was done with HLM to evaluate phase I metabolism. As shown in Figure 4A, minimal (<15%) metabolism was observed in the presence of HLM, indicating that the compound is not undergoing significant cytochrome P450-mediated metabolism. In conclusion, we developed a novel inhibitor of dependent colon cancer progression and metastasis, which is stable and potent.

3.6. Affinity and specificity of PDS-0330 binding to claudin-1

Next, we determined the binding affinity of PDS-0330 to recombinantly produced and biochemically pure Cy3-labeled human claudin-1 *in vitro* using the biophysical interaction technique MST. The equilibrium dissociation constant (Kd) of unlabeled PDS-0330 to labeled claudin-1 was 22.9 ± 3.0 μM (Fig6 A). PDS-0330 in DMSO was used for analyses, and so a control experiment was conducted to determine if DMSO bound claudin-1. No non-specific binding of DMSO to claudin-1 was detected (Fig6 B), indicating that the binding signal observed with PDS- 0330 was specific due to the inhibitor and not the vehicle.
To discern the domain on claudin-1 responsible for binding PDS-0330, we trypsinized claudin-1 to remove disordered regions at the N- and C-termini. MST measurements of PDS-0330 incubated with trypsinized and labeled claudin-1 showed no detectable binding at concentrations shown to bind wild-type claudin-1 (Fig6 C). We next determined whether the binding of PDS-0330 to claudin-1 was specific to this subtype or if PDS-0330 could generally recognize and bind the claudin fold. For this, we tested PDS-0330 binding to labeled human claudin-19 and mouse claudin-4, which have 56% and 47% sequence identity, respectively. Here, we found PDS-0330 bound both claudins but with KDs ≥100 μM, indicating lower affinity. In detail, claudin-19 bound with 157.3 ± 35.1 μM and

claudin-4 with 92.1 ± 10.5 μM of PDS-0330 (Fig6 D), suggesting that the inhibitor has higher affinity and thus selectivity for claudin-1 as compared to other family members. Lastly, to characterize PDS-0330 binding in a physiological context, we quantified its binding to claudin-1 at 37°C. Here, we measured a binding affinity of 44.9 ± 5.6 μM. However, because the generated binding curve at this temperature was sigmoidal, it was fit to the Hill-Langmuir equation, which resulted in a Hill coefficient of 4.5 (Fig6 E).

3.7. PDS-0330 inhibits claudin1-mediated signaling by interfering with its binding to Src.

In the following studies, we determined how PDS-0330 impacts the CRC cell survival and anoikis resistance. Claudin-1 has previously been found to physically associate with Src (Singh et al., 2012). The C-terminal of claudin-1 is critical for its partnering with Src, and also essential for claudin-1- mediated resistance to anoikis in a Src-Akt-Bcl-2-dependent manner as we have shown previously (Singh et al., 2012). Src signaling pathways are major regulators of the cancer cells survival, metastasis, and chemoresistance. Since, claudin-1 inhibitor was designed against the C- terminus, we hypothesized that it would inhibit claudin-1 association with Src to regulate downstream signaling and inhibit resistance to anoikis. The proximity ligation assay demonstrated that claudin-1 inhibitor, I-6 significantly interferes with the association of claudin-1 with Src (Suppl Fig 5A) and its phosphorylation (Suppl Fig5 B).

Similarly, we found that I-6 analog PDS-0330 also prevents the interaction of Src and claudin-1 (Fig 7A). SW620 cells were treated with PDS-0330 at two different concentrations (12.5μM and 25μM) or in the vehicle alone. Our results show that PDS-0330 significantly interferes with the association of Src with claudin-1 (Fig7 A). Additionally, it prevents Src phosphorylation, which impacts downstream signaling by suppressing Akt activation and by inhibiting Bcl-2 and Bcl-xL expression, interfering with claudin-1 expressing colon cancer progression (Fig7 B, Fig8 C & Suppl Fig7 E). These findings suggested that the new claudin-1 inhibitor PDS-0330 inhibits downstream signaling by blocking claudin-1 binding to Src, reducing anoikis resistance and therapy/chemoresistance (Fig 7).

3.8. PDS-0330 inhibits claudin-1 -mediated invasive and tumorigenic effects:

Next, we determined the effect of PDS-0330 on Claudin-1 mediated tumorigenesis *in-vitro* and *in- vivo.* SW480^{cld1} and SW620 cells were chosen for this study because of their strong tumorigenic/metastatic potential and high claudin-1 expression. SW480^{cld1} and SW620 cells were subjected to PDS-0330 treatment, and effects on anchorage-independent growth and cell invasion was determined. As presented in Figure 8 A&B, PDS-0330 significantly inhibited the cell invasion ($P < 0.0001$) and anchorage-independent growth (colony formation in soft agar; 65–70%) as compared to the control and 20A treated cells (taken as a negative control) (Fig8 A & B). Treatment with PDS-0330 also caused an increase in apoptosis as evidenced by an increase in apoptotic protein cleaved PARP while a decrease in anti-apoptotic proteins including Bcl2, Bcl- xL, and Survivin in claudin-1 expressing SW480^{cld1} and SW620 cells (Fig8 C & Suppl Fig7 D & E).

3.9. PDS-0330 inhibits xenograft tumor formation by claudin-1 overexpressed SW480^{cld1} and SW620 cells without showing cytotoxicity:

To determine the anti-tumorigenic role of PDS-0330 in tumor formation *in-vivo*, we performed a subcutaneous xenograft tumor generation using claudin-1 overexpressed SW480^{cld1} and SW620 cells. PDS-0330 therapy (5mg/Kg and 10mg/Kg) resulted in a significant reduction in tumor volume and weight in mice compared to vehicle treatment in both xenograft models (Fig 9 Ai, Aii, Ci, Cii & Suppl Fig6). Furthermore, at the end of the experiment, the tumors were harvested, then the IHC and immune-blot assay were performed to investigate the expression of proliferative and apoptotic markers. The results showed that in the treated group, there was an increase in apoptosis as measured by increased expression of cleaved PARP and decreased expression of BclxL and survivin, as well as reduced proliferation as measured by Ki67 (Fig9 B, D, Suppl Fig9 C, D, F & G).

To assess the drug toxicity, the mice's body weight and blood biochemistry of mice were measured. The results revealed that there were no statistically significant differences in the body weight among groups at the end of treatment (Suppl Fig7 A & B); the level of the urea nitrogen (BUN) in mice blood (Fig10 A); and aspartate transaminase (AST) levels after drug treatment were not affected (Fig10 B). These findings suggested that PDS-0330 treatment may be safe and not toxic to kidney and liver of experimental mice. However further detailed toxicology analysis remains to be determined. Overall, data showed that the PDS-0330 significantly decreased tumor growth in claudin-1 expressing colon cancer cells without causing major cytotoxicity.

In light of the significance of chemoresistance in claudin-1-mediated CRC metastasis, we further investigated the utility of PDS-0330 as an adjuvant with 5-FU or oxaliplatin in *in-vitro* and in xenograft tumor formation [6]. We observed significantly less % cell survival (CI index<1) in combination treatments (PDS-0330 and 5-FU) in claudin-1 overexpressing SW480^{cld1} and SW620 cells as compared to either treatment alone (Suppl Fig8 Ai, Aii). Additionally, we found that PDS- 0330 exhibits a synergistic effect with oxaliplatin in the inhibition of SW620 cells survival (Suppl Fig 8D). Moreover, we saw a substantial reduction in tumor volume when PDS-0330 and 5-FU were used in combination to treat an SW620 xenograft tumor, as compared to PDS-0330 or 5FU alone (Suppl Fig8 B & C). Overall, our findings suggest PDS-0330 is a potent claudin-1 inhibitor which might be useful in inhibiting its effects on tumorigenesis and chemoresistance.

3.10. PDS-0330 interferes with xenograft tumor formation in claudin-1 overexpressing chemo-resistant patient-derived xenograft (PDX) tumor:

To determine the anti-tumorigenic potential of PDS-0330 in chemo-resistant PDX tumors (Suppl Fig9 A), we implanted tumor fragments (~2 mm^3) subcutaneously in athymic nude mice. We treated the mice with PDS-0330 at two different doses (5mg/kg; once/week and 10mg/kg; once/week) for four weeks (n=5 mice/group) after confirming palpable tumor growth (3 weeks after initial transplantation). PDS-0330 reduced primary tumor growth in a statistically significant manner, as shown by: (1) mice bearing tumor images (Fig 11 Ai), (2) whole tumor images (Fig 11 Aii), and (3) H&E staining (Fig 11 D). Mean tumor volume (Fig 11 B), and tumor weight (Suppl Fig9 B) were significantly reduced; * $p < 0.05$, **

p = 0.01, *** p = 0.001, **** p = 0.0001. The tumors were also extracted at the end of the experiment, and IHC and western blot assays were used to investigate the expression of proliferative and apoptotic markers. The results showed that in the treated group, there was an increase in apoptosis as measured by increased expression of cleaved PARP and decreased expression of anti-apoptotic proteins Bcl-xL and survivin, as well as decreased proliferation as measured by Ki67 (Fig 11 C, D, Suppl Fig9 E, H & I), suggesting efficacy of PDS-0330 in chemo-resistant colon cancer patients' tumors.

4.0. Discussion:

Despite advances in chemotherapeutic options, CRC remains one of the leading causes of cancer deaths worldwide [4, 29]. The increasing prevalence of CRC necessitates the search for novel treatment approaches. To develop more specific and effective agents, it is imperative that we fully understand the molecular mechanism(s) governing CRC development and progression. In this context, several studies, including ours, have shown that, in human CRC patient samples, the tight junction protein claudin-1 is significantly overexpressed, with dysregulated cellular localization [6, 30, 31]. In normal epithelial cells, claudin-1 helps to keep the barrier function intact [32]. However, in cancers, its overexpression promotes the cellular transformation, invasion, epithelial- to-mesenchymal transition (EMT), and metastasis [6, 31, 33–36]. Claudin-1 also plays a significant role in increasing anoikis resistance in CRC progression, and that resistance to anoikis might predict the capacity to produce metastatic lesions [19]. Though, much work has been devoted in investigating claudin-1 function and regulation in cancer, very little known about its promising potential as a therapeutic target. One study has demonstrated that claudin-1 targeting using a monoclonal antibody led to reduced proliferation and survival of CRC cells [15], indicating that claudin-1 may be a promising target for CRC treatment. While the oncogenic activities of claudin-1 make it a promising therapeutic target, no claudin-1 inhibitors are currently available for clinical use. The objective of this study was to develop and evaluate the efficacy of a small- molecule inhibitor of claudin-1 as a therapeutic modality for CRC.

As the crystal structure of claudin-1 is unknown, we used an *in-silico* protein folding program, YASARA, to identify potential sites for claudin-1 inhibitor binding. In a high throughput virtual screen, the top 10 candidates were selected as a hit with the best binding energies that bound to Site#3 (targeting near c-terminal domain; the most accessible pocket) and used for further screening by anoikis (induction of apoptosis in epithelial cells by denying the appropriate cell- matrix interaction) assay. Among them, the I-6 compound was identified as a promising hit against claudin-1 expressing colon cancer cells, which are highly invasively/metastatic. Thus, we postulated that I-6 could be able to prevent colon cancer growth progression that are characterized by upregulated claudin-1 expression and its mediated signaling. Notably, the binding of I-6 to putative claudin-1 sites and hence suppression of anoikis resistance would provide information about its mode of action.

I-6 had high binding efficacy to claudin-1 and effectively inhibited claudin-1-mediated CRC growth; however, it was rapidly metabolized, with only 49% of the drug remaining after 60 min. and had a low bioavailability (<1%). The findings of these *in-vitro* drug-

metabolism and *in-vivo* PK investigations of I-6 give the requisite incentive for additional structural modification of this pharmacophore in order to improve stability and pave the way for the logical development of its analogs. Therefore, we synthesized I-6 analogs with increased stability. Of these analogs, PDS- 0330 had the highest stability, with a low plasma clearance (CL) and a long plasma half-life (t1/2). It was also most effective in inhibiting claudin-1-mediated colon cancer growth and invasion *in- vitro* and *in-vivo*. In claudin-1 expressing colon cancer cells, PDS-0330 reduced anoikis resistance and inhibited proliferation by blocking the association of claudin-1 and Src; no effects were observed in normal intestinal cells. PDS-0330 was also found to inhibit tumor growth in xenograft models without any observable effects on kidney or liver function. Notably, it has been demonstrated that claudin-1 knockdown increased chemosensitivity and decreased cell proliferation, migration, and wound healing, which is noteworthy considering the role that claudin- 1 plays in chemoresistance [37]. Noticeably, our findings found considerable synergy in the anticancer effects of 5-FU and oxaliplatin with PDS-03330 *in vitro* and in the prevention of tumor formation in claudin-1 expressed xenograft mice model, which is important given the significance of chemoresistance in claudin-1-mediated CRC metastases. Altogether, our data showed that PDS- 0330 displayed antitumor and chemosensitizer activity with favorable pharmacokinetic features. Moreover, recent research has revealed complex protein partnering as a possible pathway for dysregulated oncogenic signaling that leads to CRC aggressiveness [19, 38, 39]. These findings strongly suggest that dysregulated claudin-1 expression plays a role in promoting Src and other signaling pathways that have been linked to changes in homotypic adhesion, angiogenesis, tumor cell invasiveness, tumor growth, and anoikis, all of which play an important role in the development of the metastatic phenotype [6, 19]. It has been extensively investigated that the Src family kinase, Src, is highly expressed, commonly mutated in colorectal cancer, and confers anoikis resistance in a variety of epithelial cells [40]. Our earlier research shown that claudin-1- associated resistance to anoikis relies on Src activation, which in turn affects Akt phosphorylation and Bcl-2 expression [41, 42]. Additionally, claudin-1 interacts with Src/p-Src in a multiprotein complex as a result of dysregulated and increased expression under specific clinical situations, and loss of the association between claudin-1 and Src/p-Src reduces the resistance to anoikis in accordance with our previously reported findings [19]. We anticipate this is the reason why PDS- 0330 exclusively affects colon cancer cells (*in-vitro and in-vivo*) and has no effect on normal cells in vitro, has no cytotoxic effects on the liver and kidney, and has no effect on mice behavior or weight in vivo as well.

Despite the promising potential of kinase inhibitors in the treatment of CRC, preclinical and clinical investigations have revealed that only about 20% of patients with metastatic colorectal react to currently available targeted drugs, justifying the search for new therapeutic approaches [43–45]. In addition to this, studies investigating this calamitous failure of effective treatment of aggressive cancer have also revealed that, given the existence of complex cross-talks among different kinase cascades in promoting CRC malignancy, targeting only one pathway would result in an undesirable imbalance between the interacting oncogenic kinases and activation of compensatory signaling, resulting in apoptosis evasion [46]. As a result, blocking many signaling kinases that are elevated in aggressive CRC can be cautious (and effective) in limiting cancer cell growth and viability [45, 47], which

is the central notion of this study. Notably, Src tyrosine kinase has long been linked to treatment resistance in metastatic CRC. However, in the individuals that were treated, Src monotherapy failed to produce a meaningful composite outcome of overall survival [48]. We hypothesize that our newly discovered compound, PDS-0330, not only disrupts the CRC -specific Claudin-1 association with, Src but also interferes with other dependent oncogenic signaling. Therefore, in the following study, we will emphasize the underneath detailed molecular signaling of this compound that results in the prevention of colon cancer cell proliferation and tumorigenesis. Here, throughout the entire investigation, PDS-0330 appears to be a novel, potent, and selective claudin-1 inhibitor that particularly impedes the development of claudin-1 overexpressed CRC.

Our biophysical binding studies of PDS-0330 to claudins show that it binds human claudin-1 selectively compared to human claudin-19 and mouse claudin-4, indicating that claudin-1 likely possesses regions with unique amino acid sequences that are somewhat specifically recognized by PDS-0330. Binding affinities of PDS-0330 to other claudin subtypes was ~4- fold lower than claudin-1. Further, our data suggest that PDS-0330 likely binds the C-terminus of claudin-1, as this region is unstructured and susceptible to trypsin digestion (data not shown). Generally, claudins have numerous phosphorylation sites at C-terminal residues [49]. Human claudin-1 is predicted to have 8 phosphorylation sites on its C-terminus, while human claudin-19 and mouse claudin-4 are predicted to each have only 3 [50]. Binding of PDS-0330 may thus be altered upon this post-translational modification. Finally, our binding data at 37°C showed similar binding affinity to data collected at room temperature but had a Hill coefficient of ~5. These results suggest that PDS-0330 binds claudins with positive cooperativity *in vivo*. In sum, we hypothesize that PDS-0330 targets phosphorylated amino acids or amino acids capable of being phosphorylated (Ser, Thr, Tyr) as part of its binding mechanism, which would explain its higher affinity for human claudin-1 over other claudins tested and the loss of PDS-0330 binding to claudin-1 resulting from trypsinization of its C-terminus. Further studies are needed to validate this idea.

In summary, this work addresses a critical clinical need by discovering and providing preclinical testing for a new small molecule inhibitor against claudin-1. This inhibitor, PDS-0330, has the potential to reduce the impact of claudin-1-dependent CRC metastasis and chemoresistance. Our data shows that PDS-0330 specifically inhibits binding of claudin-1 to Src thus inhibiting the resistance of anoikis, and shows anti-invasive and anti-tumorigenic potential in claudin-1 overexpressed cells. These outcomes provide strong preclinical rationale for the development and use of claudin-1 inhibitors in colon cancer treatment.

Supplementary Material

Refer to Web version on PubMed Central for supplementary material.

Acknowledgement:

This study was supported by BX002086 (VA merit) to P.D and CA250383 (NIH/NCI) to P.D and CRH and DK124095 and BX002761 (VA merit) to ABS.

References:

1. Miller KD, Nogueira L, Devasia T, Mariotto AB, Yabroff KR, Jemal A et al. Cancer treatment and survivorship statistics, 2022. CA Cancer J Clin 2022.
2. Siegel RL, Miller KD, Fuchs HE, Jemal A. Cancer statistics, 2022. CA Cancer J Clin 2022; 72: 7–33. [PubMed: 35020204]
3. Siegel RL, Miller KD, Jemal A. Cancer statistics, 2019. CA Cancer J Clin 2019; 69: 7–34. [PubMed: 30620402]
4. Xie YH, Chen YX, Fang JY. Comprehensive review of targeted therapy for colorectal cancer. Signal Transduct Target Ther 2020; 5: 22. [PubMed: 32296018]
5. Modest DP, Rivera F, Bachet JB, de Braud F, Pietrantonio F, Koukakis R et al. Panitumumab-based maintenance after oxaliplatin discontinuation in metastatic colorectal cancer: A retrospective analysis of two randomised trials. Int J Cancer 2019; 145: 576–585. [PubMed: 30614531]
6. Dhawan P, Singh AB, Deane NG, No Y, Shiou SR, Schmidt C et al. Claudin-1 regulates cellular transformation and metastatic behavior in colon cancer. J Clin Invest 2005; 115: 1765–1776. [PubMed: 15965503]
7. Furuse M, Fujita K, Hiiragi T, Fujimoto K, Tsukita S. Claudin-1 and −2: novel integral membrane proteins localizing at tight junctions with no sequence similarity to occludin. J Cell Biol 1998; 141: 1539–1550. [PubMed: 9647647]
8. Tsukita S, Furuse M, Itoh M. Multifunctional strands in tight junctions. Nat Rev Mol Cell Biol 2001; 2: 285–293. [PubMed: 11283726]
9. Offner S, Hekele A, Teichmann U, Weinberger S, Gross S, Kufer P et al. Epithelial tight junction proteins as potential antibody targets for pancarcinoma therapy. Cancer Immunol Immunother 2005; 54: 431–445. [PubMed: 15750830]
10. Krause G, Winkler L, Mueller SL, Haseloff RF, Piontek J, Blasig IE. Structure and function of claudins. Biochim Biophys Acta 2008; 1778: 631–645. [PubMed: 18036336]
11. Lal-Nag M, Morin PJ. The claudins. Genome Biol 2009; 10: 235. [PubMed: 19706201]
12. Gunzel D, Fromm M. Claudins and other tight junction proteins. Compr Physiol 2012; 2: 1819–1852. [PubMed: 23723025]
13. Grone J, Weber B, Staub E, Heinze M, Klaman I, Pilarsky C et al. Differential expression of genes encoding tight junction proteins in colorectal cancer: frequent dysregulation of claudin-1, −8 and −12. Int J Colorectal Dis 2007; 22: 651–659. [PubMed: 17047970]
14. Huo Q, Kinugasa T, Wang L, Huang J, Zhao J, Shibaguchi H et al. Claudin-1 protein is a major factor involved in the tumorigenesis of colorectal cancer. Anticancer Res 2009; 29: 851–857. [PubMed: 19414319]
15. Cherradi S, Ayrolles-Torro A, Vezzo-Vie N, Gueguinou N, Denis V, Combes E et al. Antibody targeting of claudin-1 as a potential colorectal cancer therapy. J Exp Clin Cancer Res 2017; 36: 89. [PubMed: 28659146]
16. Singh AB, Sharma A, Dhawan P. Claudin family of proteins and cancer: an overview. J Oncol 2010; 2010: 541957.
17. Miwa N, Furuse M, Tsukita S, Niikawa N, Nakamura Y, Furukawa Y. Involvement of claudin-1 in the beta-catenin/Tcf signaling pathway and its frequent upregulation in human colorectal cancers. Oncol Res 2001; 12: 469–476. [PubMed: 11939410]
18. Pope JL, Bhat AA, Sharma A, Ahmad R, Krishnan M, Washington MK et al. Claudin-1 regulates intestinal epithelial homeostasis through the modulation of Notch-signalling. Gut 2014; 63: 622–634. [PubMed: 23766441]
19. Singh AB, Sharma A, Dhawan P. Claudin-1 expression confers resistance to anoikis in colon cancer cells in a Src-dependent manner. Carcinogenesis 2012; 33: 2538–2547. [PubMed: 22941059]
20. Frisch SM, Francis H. Disruption of epithelial cell-matrix interactions induces apoptosis. J Cell Biol 1994; 124: 619–626. [PubMed: 8106557]

21. Huang J, Li J, Qu Y, Zhang J, Zhang L, Chen X et al. The expression of claudin 1 correlates with beta- catenin and is a prognostic factor of poor outcome in gastric cancer. Int J Oncol 2014; 44: 1293–1301. [PubMed: 24535143]
22. Fatima I, Barman S, Uppada J, Chauhan S, Rauth S, Rachagani S et al. MASTL regulates EGFR signaling to impact pancreatic cancer progression. Oncogene 2021; 40: 5691–5704. [PubMed: 34331012]
23. Fatima I, Chandra V, Saxena R, Manohar M, Sanghani Y, Hajela K et al. 2,3-Diaryl-2H-1-benzopyran derivatives interfere with classical and non-classical estrogen receptor signaling pathways, inhibit Akt activation and induce apoptosis in human endometrial cancer cells. Mol Cell Endocrinol 2012; 348: 198–210. [PubMed: 21878365]
24. Sato T, Stange DE, Ferrante M, Vries RG, Van Es JH, Van den Brink S et al. Long-term expansion of epithelial organoids from human colon, adenoma, adenocarcinoma, and Barrett's epithelium. Gastroenterology 2011; 141: 1762–1772. [PubMed: 21889923]
25. Fatima I, El-Ayachi I, Playa HC, Alva-Ornelas JA, Khalid AB, Kuenzinger WL et al. Simultaneous Multi-Organ Metastases from Chemo-Resistant Triple-Negative Breast Cancer Are Prevented by Interfering with WNT-Signaling. Cancers (Basel) 2019; 11.
26. Vecchio AJ, Stroud RM. Claudin-9 structures reveal mechanism for toxin-induced gut barrier breakdown. Proc Natl Acad Sci U S A 2019; 116: 17817–17824. [PubMed: 31434788]
27. Baarnhielm C, Dahlback H, Skanberg I. In vivo pharmacokinetics of felodipine predicted from in vitro studies in rat, dog and man. Acta pharmacologica et toxicologica (Comparative Study In Vitro) 1986; 59: 113–122.
28. Smith R, Jones RD, Ballard PG, Griffiths HH. Determination of microsome and hepatocyte scaling factors for in vitro/in vivo extrapolation in the rat and dog. Xenobiotica; the fate of foreign compounds in biological systems 2008; 38: 1386–1398. [PubMed: 18988082]
29. Hossain MS, Karuniawati H, Jairoun AA, Urbi Z, Ooi J, John A et al. Colorectal Cancer: A Review of Carcinogenesis, Global Epidemiology, Current Challenges, Risk Factors, Preventive and Treatment Strategies. Cancers (Basel) 2022; 14.
30. Dos Reis PP, Bharadwaj RR, Machado J, Macmillan C, Pintilie M, Sukhai MA et al. Claudin 1 overexpression increases invasion and is associated with aggressive histological features in oral squamous cell carcinoma. Cancer 2008; 113: 3169–3180. [PubMed: 18991282]
31. Leotlela PD, Wade MS, Duray PH, Rhode MJ, Brown HF, Rosenthal DT et al. Claudin-1 overexpression in melanoma is regulated by PKC and contributes to melanoma cell motility. Oncogene 2007; 26: 3846–3856. [PubMed: 17160014]
32. Gunzel D, Yu AS. Claudins and the modulation of tight junction permeability. Physiol Rev 2013; 93: 525–569. [PubMed: 23589827]
33. Yoon CH, Kim MJ, Park MJ, Park IC, Hwang SG, An S et al. Claudin-1 acts through c-Abl-protein kinase Cdelta (PKCdelta) signaling and has a causal role in the acquisition of invasive capacity in human liver cells. J Biol Chem 2010; 285: 226–233. [PubMed: 19897486]
34. Oku N, Sasabe E, Ueta E, Yamamoto T, Osaki T. Tight junction protein claudin-1 enhances the invasive activity of oral squamous cell carcinoma cells by promoting cleavage of laminin-5 gamma2 chain via matrix metalloproteinase (MMP)-2 and membrane-type MMP-1. Cancer Res 2006; 66: 5251–5257. [PubMed: 16707450]
35. Tokes AM, Kulka J, Paku S, Szik A, Paska C, Novak PK et al. Claudin-1, −3 and −4 proteins and mRNA expression in benign and malignant breast lesions: a research study. Breast Cancer Res 2005; 7: R296–305. [PubMed: 15743508]
36. Bhat AA, Ahmad R, Uppada SB, Singh AB, Dhawan P. Claudin-1 promotes TNF-alpha-induced epithelial-mesenchymal transition and migration in colorectal adenocarcinoma cells. Exp Cell Res 2016; 349: 119–127. [PubMed: 27742576]
37. Visco ZR, Sfakianos G, Grenier C, Boudreau MH, Simpson S, Rodriguez I et al. Epigenetic Regulation of Claudin-1 in the Development of Ovarian Cancer Recurrence and Drug Resistance. Front Oncol 2021; 11: 620873.
38. Malki A, ElRuz RA, Gupta I, Allouch A, Vranic S, Al Moustafa AE. Molecular Mechanisms of Colon Cancer Progression and Metastasis: Recent Insights and Advancements. Int J Mol Sci 2020; 22.

39. Koveitypour Z, Panahi F, Vakilian M, Peymani M, Seyed Forootan F, Nasr Esfahani MH et al. Signaling pathways involved in colorectal cancer progression. Cell Biosci 2019; 9: 97. [PubMed: 31827763]
40. Chen J. Is Src the key to understanding metastasis and developing new treatments for colon cancer? Nat Clin Pract Gastroenterol Hepatol 2008; 5: 306–307. [PubMed: 18477987]
41. Galante JM, Mortenson MM, Bowles TL, Virudachalam S, Bold RJ. ERK/BCL-2 pathway in the resistance of pancreatic cancer to anoikis. J Surg Res 2009; 152: 18–25. [PubMed: 19062038]
42. Coll ML, Rosen K, Ladeda V, Filmus J. Increased Bcl-xL expression mediates v-Src-induced resistance to anoikis in intestinal epithelial cells. Oncogene 2002; 21: 2908–2913. [PubMed: 11973652]
43. Nalli M, Puxeddu M, La Regina G, Gianni S, Silvestri R. Emerging Therapeutic Agents for Colorectal Cancer. Molecules 2021; 26.
44. De Roock W, De Vriendt V, Normanno N, Ciardiello F, Tejpar S. KRAS, BRAF, PIK3CA, and PTEN mutations: implications for targeted therapies in metastatic colorectal cancer. Lancet Oncol 2011; 12: 594–603. [PubMed: 21163703]
45. Garcia-Aranda M, Redondo M. Targeting Receptor Kinases in Colorectal Cancer. Cancers (Basel) 2019; 11.
46. Fang JY, Richardson BC. The MAPK signalling pathways and colorectal cancer. Lancet Oncol 2005; 6: 322–327. [PubMed: 15863380]
47. Ahronian LG, Corcoran RB. Effective MAPK Inhibition is critical for therapeutic responses in colorectal cancer with BRAF mutations. Mol Cell Oncol 2016; 3: e1048405.
48. Brooks HD, Glisson BS, Bekele BN, Johnson FM, Ginsberg LE, El-Naggar A et al. Phase 2 study of dasatinib in the treatment of head and neck squamous cell carcinoma. Cancer 2011; 117: 2112–2119. [PubMed: 21523723]
49. Van Itallie CM, Anderson JM. Phosphorylation of tight junction transmembrane proteins: Many sites, much to do. Tissue Barriers 2018; 6: e1382671.
50. Blom N, Sicheritz-Ponten T, Gupta R, Gammeltoft S, Brunak S. Prediction of post-translational glycosylation and phosphorylation of proteins from the amino acid sequence. Proteomics 2004; 4: 1633–1649. [PubMed: 15174133]

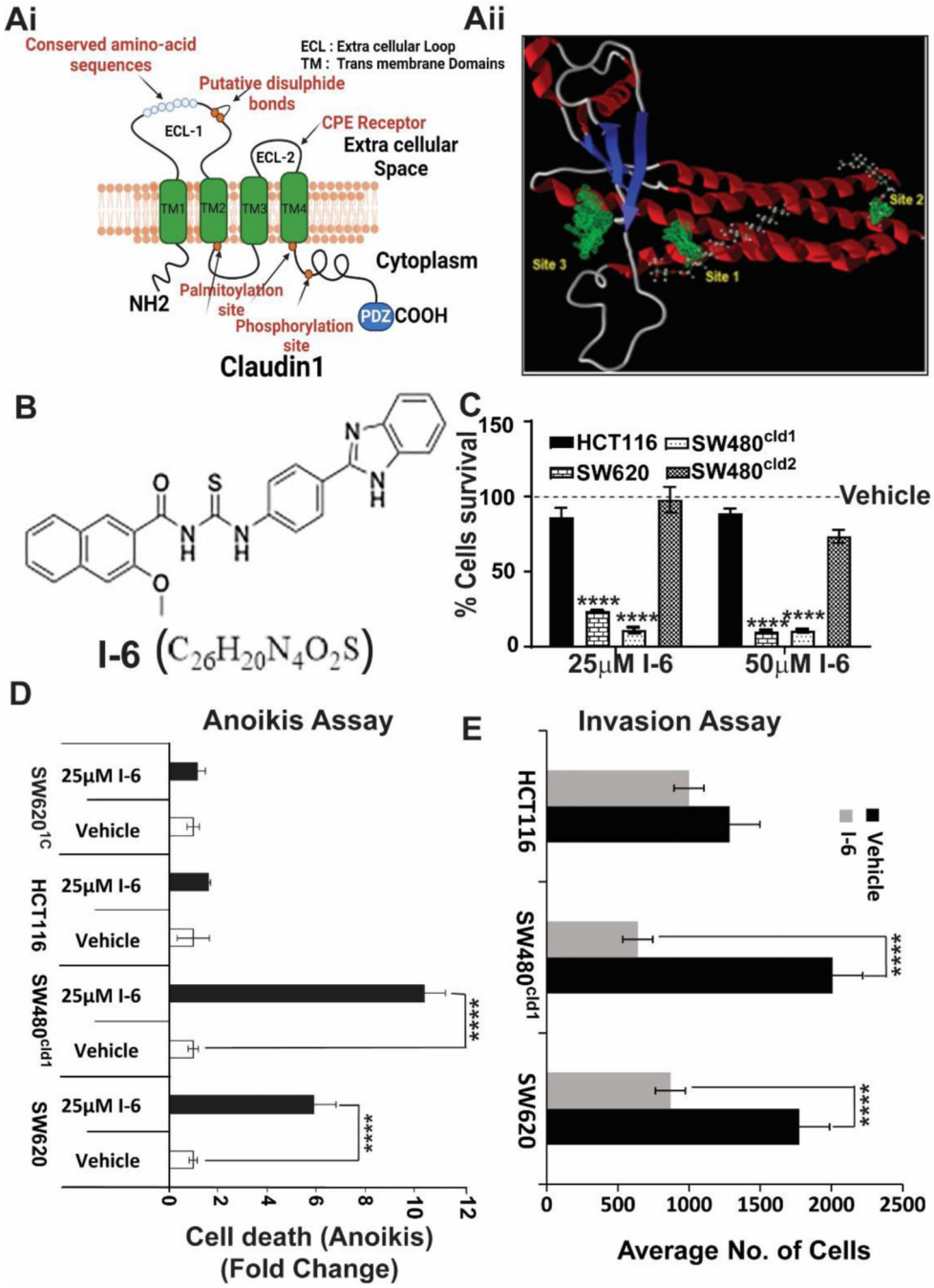

Figure 1. I-6, a claudin-1 inhibitor, interferes with cell survival, resistance to anoikis and invasion.

(Ai) Claudin-1 structure.; (Aii) *in-silico* 3D structure of claudin-1 as well as cavities that small compounds can target.; (B) Chemical structure of compound I-6.; (C) I-6 (25 & 50μM) significantly decreases cell viability only in the claudin-1 overexpressed SW620 and SW480^{cld1} cells while showing no significant impact on the HCT116 and SW480^{cld2} cells ($P<0.001$).; (D) I-6 dramatically affects anoikis resistance only in the claudin-1 overexpressed SW620 and SW480^{cld1} cells while having no impact on the claudin-1 deficient SW620^{1C} and HCT116 cells.; (E) I-6 suppresses invasion in claudin-1

overexpressed SW620 and SW480^{cld1} cells but has no effect in claudin-1 deficient HCT116 cells. Results analyzed by 2way ANOVA. For graphs, data represent mean ± SD; *, P < 0.05; **, P < 0.01; ***, P < 0.001 & ****, P < 0.0001.

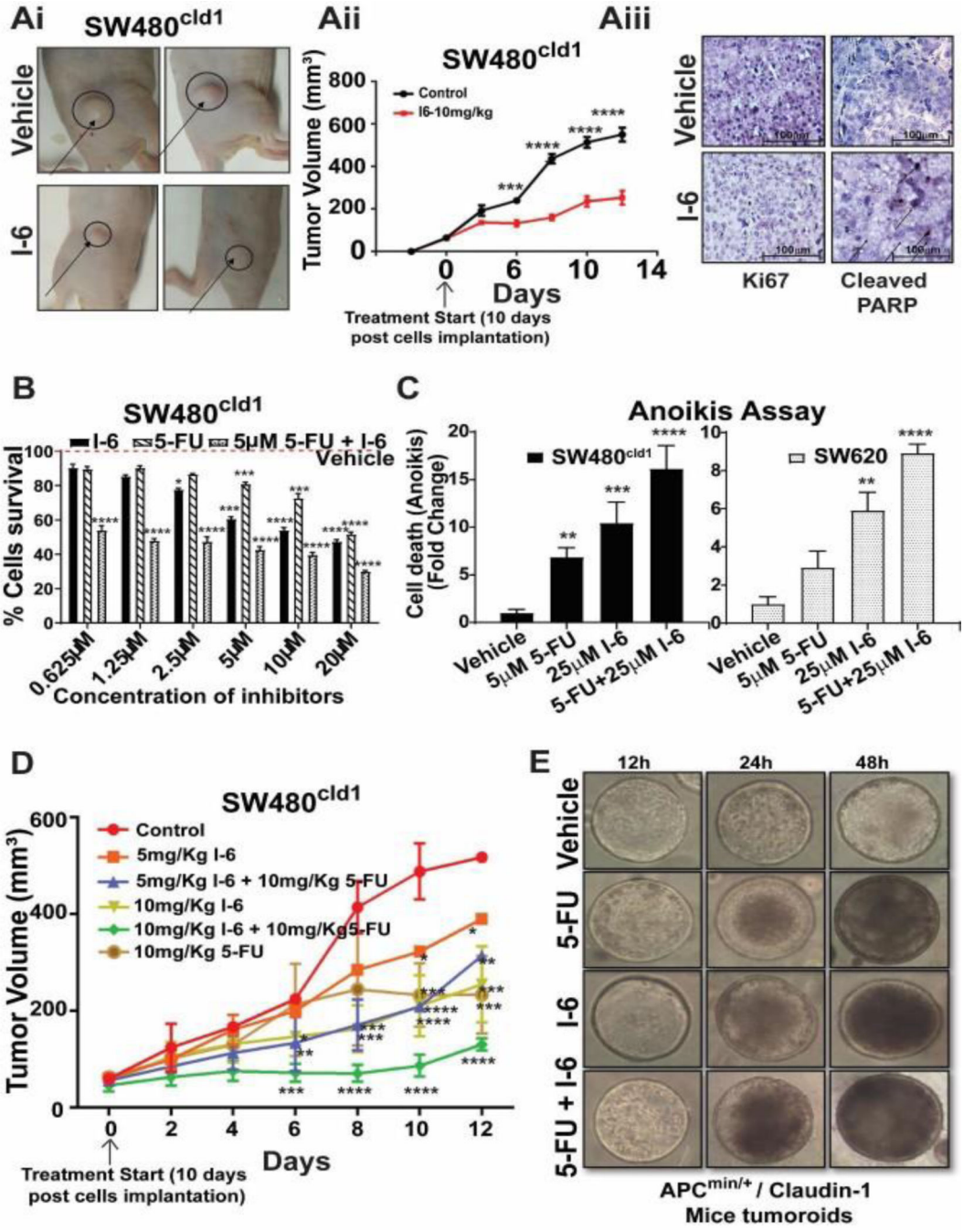

Figure 2. The anti-tumorigenic potential of I-6.

(Ai-Aiii) The development of flank xenograft tumors after subcutaneous injection (n = 5 mice per group) was compared between control and I-6 (10mg/kg) treated claudin-1 overexpressed SW480^{cld1} cells injected nude mice (Ai).; After week 3, I-6 treatment (10mg/Kg) significantly prevent the development of xenograft tumor (Aii).; Immunohistochemical analysis (scale equals 100 μm) of proliferation marker (Ki67) and apoptotic marker (cleaved PARP) were observed in respective tumor sections (Aiii).; (B-E) Inhibitor I-6 acts as an adjuvant in co-treatment with 5-FU for anti- CRC therapy. I-6 shows

(0.625μM-20μM) synergistic effect with 5-FU (5μM) in preventing claudin-1 overexpressed SW480^{cld1} cells growth (B).; in inhibiting anoikis resistance in claudin-1 overexpressed SW480^{cld1} and SW620 cells (C).; inhibiting the development of claudin-1 overexpressed SW480^{cld1} xenograft tumor in nude mice (D).; in inducing apoptosis in colon tumoroids from the APC$^{min/+}$ / claudin-1 mice (E). Results analyzed by 2way ANOVA. For graphs, data represent mean ± SD; *, P < 0.05; **, P < 0.01; ***, P < 0.001 & ****, P < 0.0001.

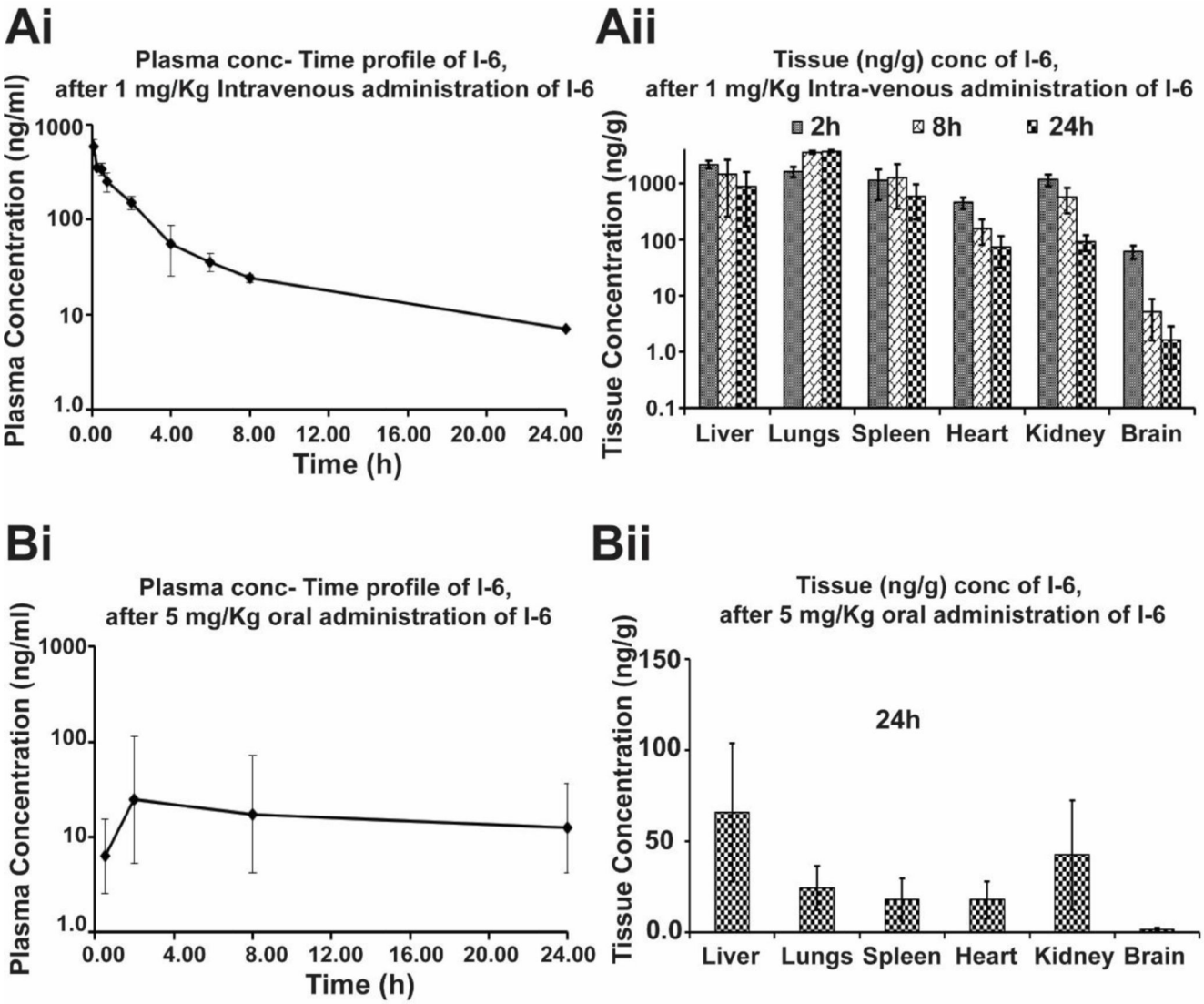

Figure 3. Pharmacokinetics (PK) and bio-distribution studies of I-6.

(Ai & Bi) Plasma concentration (ng/ml) profile of I-6 following intravenous (1mg/kg) or oral (5mg/kg) treatment (mean ± SD, n=5).; (Aii & Bii) Tissue concentrations of I-6 following intravenous (1mg/kg) or oral (5mg/kg) administration (mean ± SD, n=5).

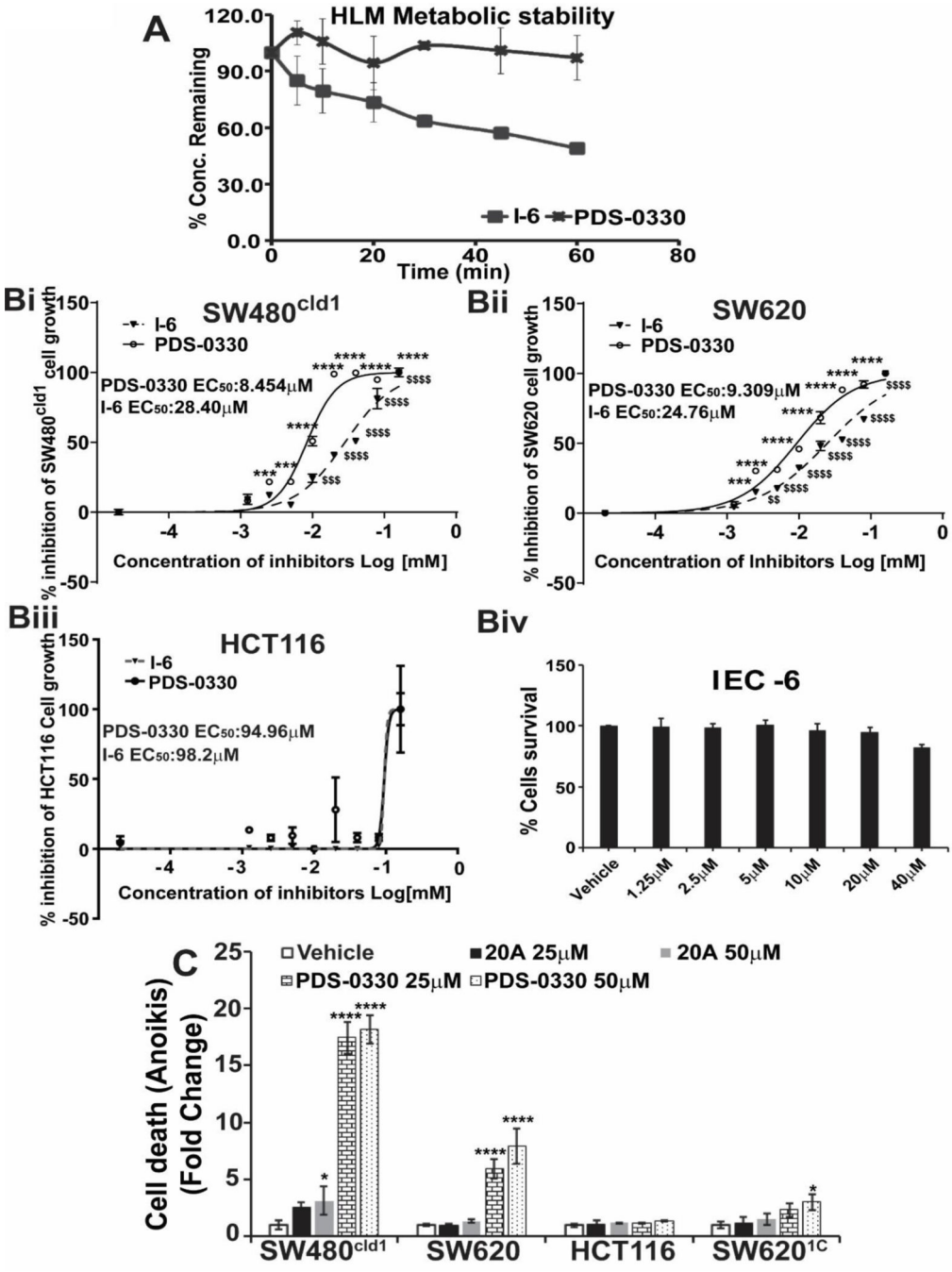

Figure 4. PDS-0330 analog is better than I-6.

(A) Evaluate the Phase I metabolism of I-6 and PDS-0330 in human liver microsomes. The result of the metabolic stability study was expressed as the percentage of the drug remaining.; (Bi-Biv) Cell viability was assessed after 72 hours of treatment with various inhibitor concentrations (PDS-0330 and I-6), and the EC_{50} was calculated using a graph pad prism in claudin-1 overexpressed $SW480^{cld1}$ and SW620 cells in claudin-1 deficient cells HCT116 and normal IEC-6 cells.; (C) PDS-0330 significantly inhibits anoikis resistance, specifically in the claudin-1 overexpressed $SW480^{cld1}$ and SW620 cells, while not affecting

the claudin-1 deficient SW620^{1C} and HCT116 cells. Compound 20A is used as a negative control. Results analyzed by 2way ANOVA. For graphs, data represent mean ± SD; *, $P < 0.05$; **, $P < 0.01$; ***, $P < 0.001$ & ****, $P < 0.0001$.

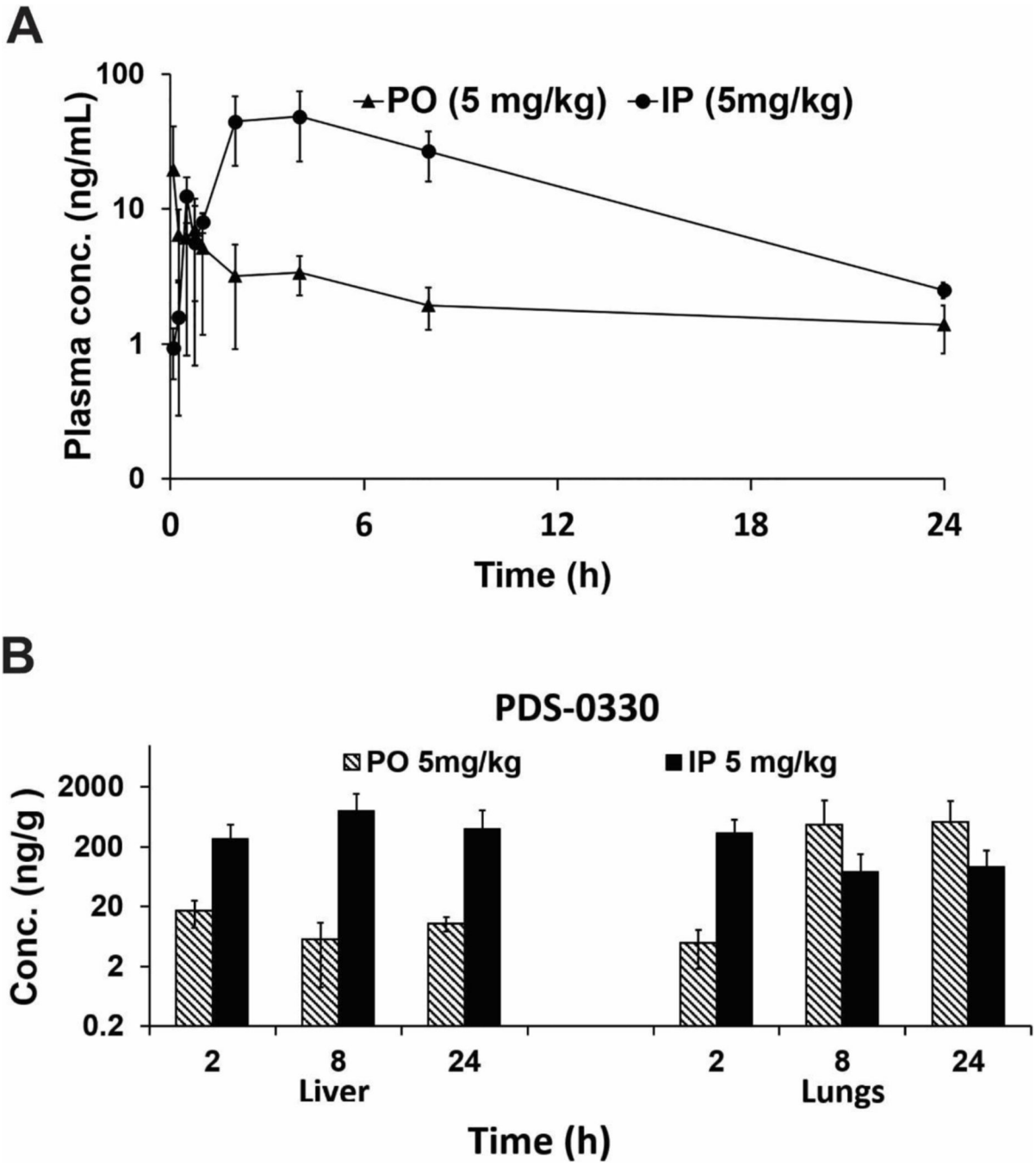

Figure 5. Pharmacokinetics (PK) and bio-distribution studies of PDS-0330.

(A) PDS-0330 plasma concentration profile following oral and IP doses of 5mg/kg both (mean ± SD, n=5); (B) Tissue concentrations of PDS-0330 following oral (5mg/kg) or IP (5mg/kg) administration (mean ± SD, n=5).

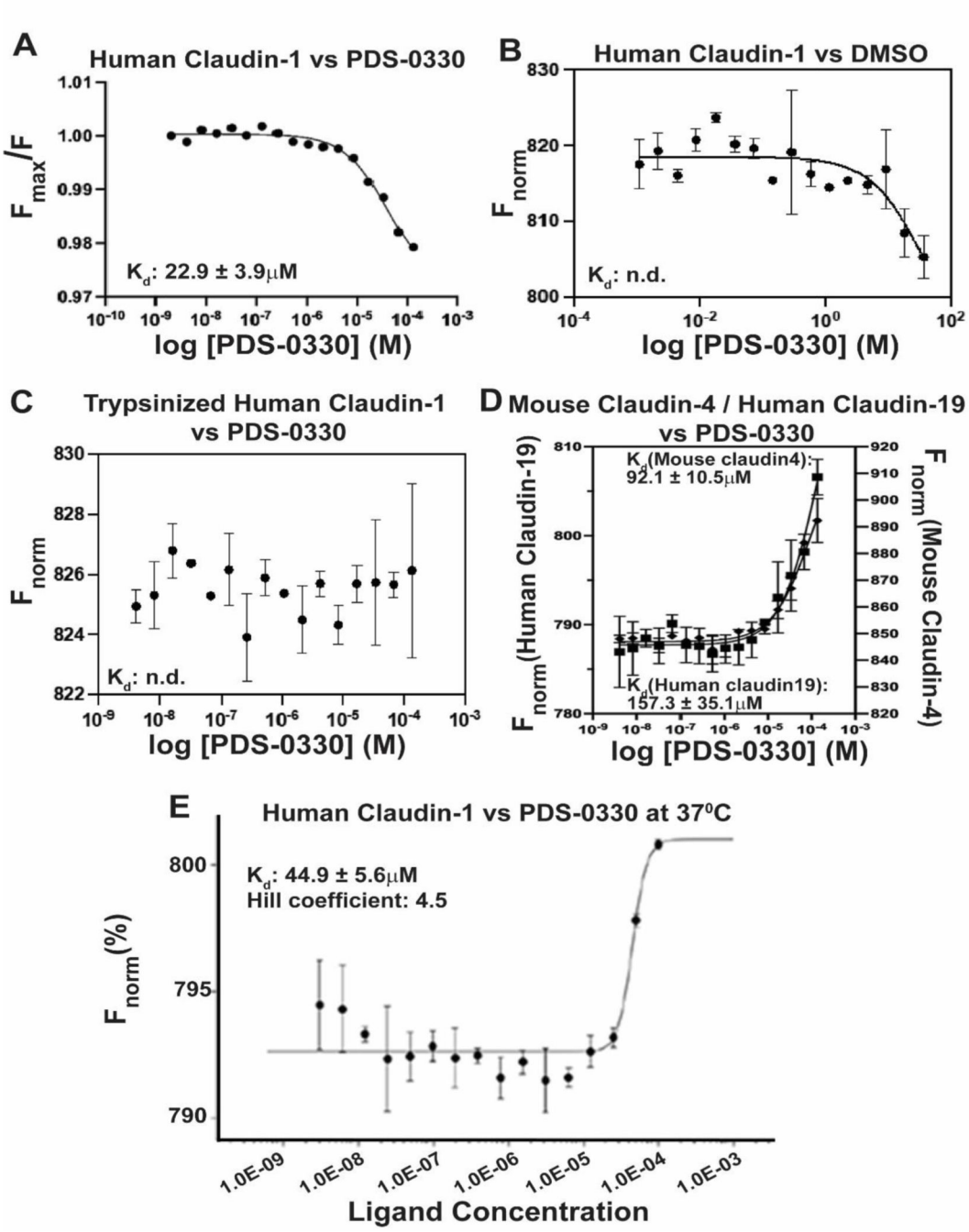

Figure 6. Microscale thermophoresis (MST) for the binding of PDS-0330.

Microscale thermophoresis for the binding of PDS-0330 to (A) human claudin 1; (B) DMSO (no claudin 1 added); (C) Cy3 labeled trypsinized human claudin 1; (D) human claudin 19/mouse claudin-4; and (E) human claudin-1 at 37°C. In panel A, Fmax/F corresponds to the ratio between the fluorescence intensities at the highest and the lowest concentrations of PDS-0330. The estimated value of the dissociation constant is 22.9 ± 3.0 μM. DMSO concentration (panel B) varied from 36.5M-1.1M, which is similar to the concentrations of DMSO carried over at the different PDS concentrations. Binding data of human claudin 19

and mouse claudin 4 (panel D) are represented on the left and right Y-axis, respectively. The affinity and the standard error for the MST measurement with human claudin-1 (panel A) were estimated from eight independent acquisitions. For all other measurements, the affinity was estimated from duplicate acquisitions. The concentration of the PDS-0330 inhibitor varied from 135 μM – 4.1 nM in all experiments. The concentration of all claudins was fixed at 1 μM. The temperature for all measurements in panels A-D was fixed at 25 °C.

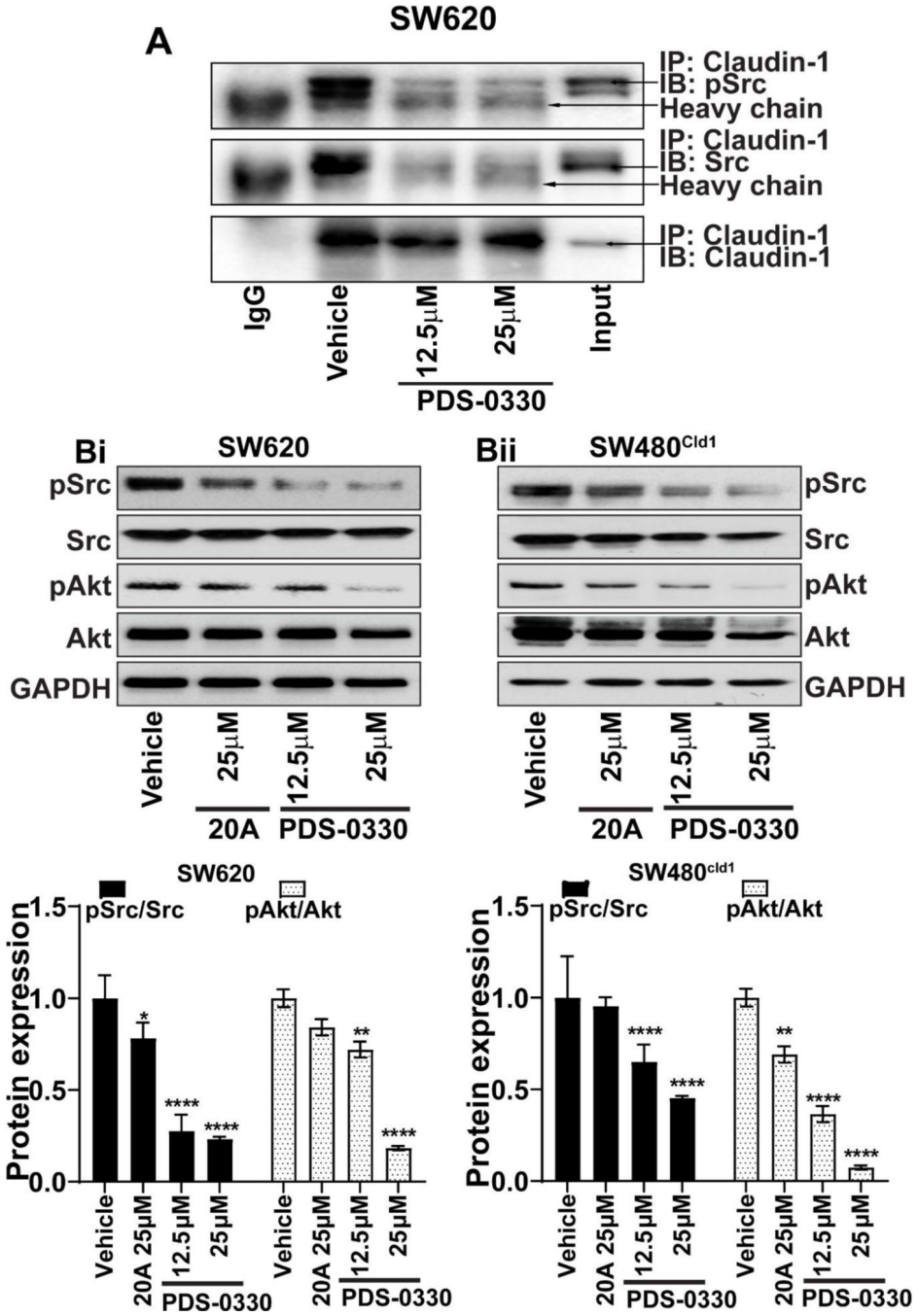

Figure 7. PDS-0330 Interferes with claudin-1 and Src binding and affects downstream molecules.

(A) Total cell lysate from the vehicle and PDS-0330 treated (12.5μM and 25μM) SW620 cells were immunoprecipitated using anti-claudin-1 antibody followed by immunoblotting with anti-pSrc, anti-Src and/or anti-claudin-1 antibody, respectively.; (B) Expression of pSrc, Src, pAkt, and Akt and its densitometry were observed in claudin-1 overexpressed SW620 and SW480^{cld1} cells upon 20A (25μM) and PDS-0330 (12.5 and 25μM) treatment by immunoblotting. Results analyzed by 2 way ANOVA. For graphs, data represent mean ± SD; *, P < 0.05; **, P < 0.01; ***, P < 0.001 & ****, P < 0.0001.

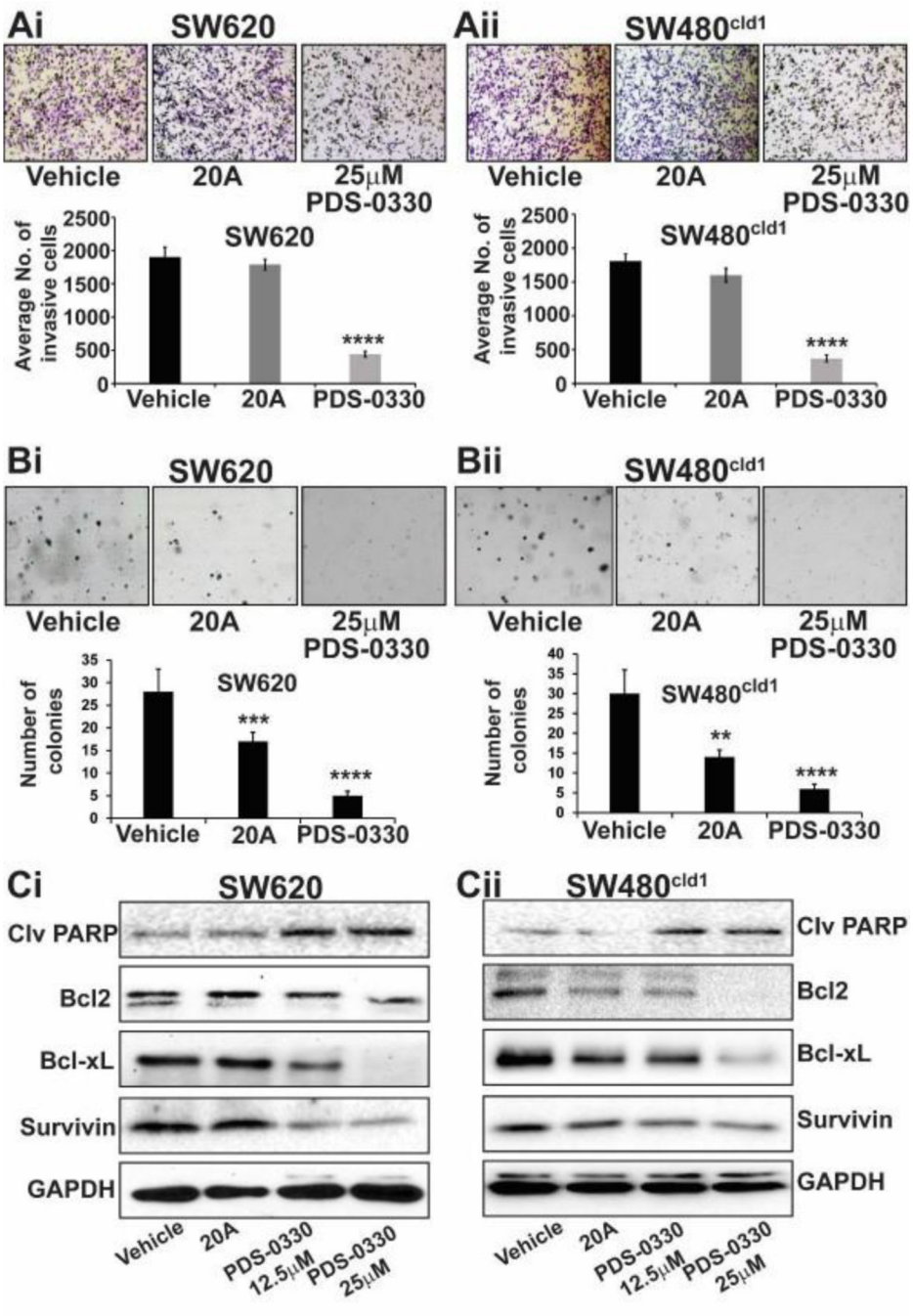

Figure 8. Anti-invasive and anti-tumorigenic potential of PDS-0330.

(A&B) The ability of PDS-0330 (25μM) to prevent invasion and interfere with colony formation in soft agar assays in claudin-1 overexpressed SW620 and SW480^{cld1} cells were used to determine its anti-invasive and anti-tumorigenic potential. Compound 20A (25μM) was taken as negative control; (Ci & ii) Apoptotic marker cleaved PARP and anti-apoptotic markers Bcl2, BclxL, and survivin were observed in claudin-1 overexpressed SW620 and SW480^{cld1} cells upon 20A (25μM) and PDS-0330 (12.5 and 25μM) treatment

by immunoblotting. Results analyzed by 2way ANOVA. For graphs, data represent mean ± SD; *, $P < 0.05$; **, $P < 0.01$; ***, $P < 0.001$ & ****, $P < 0.0001$.

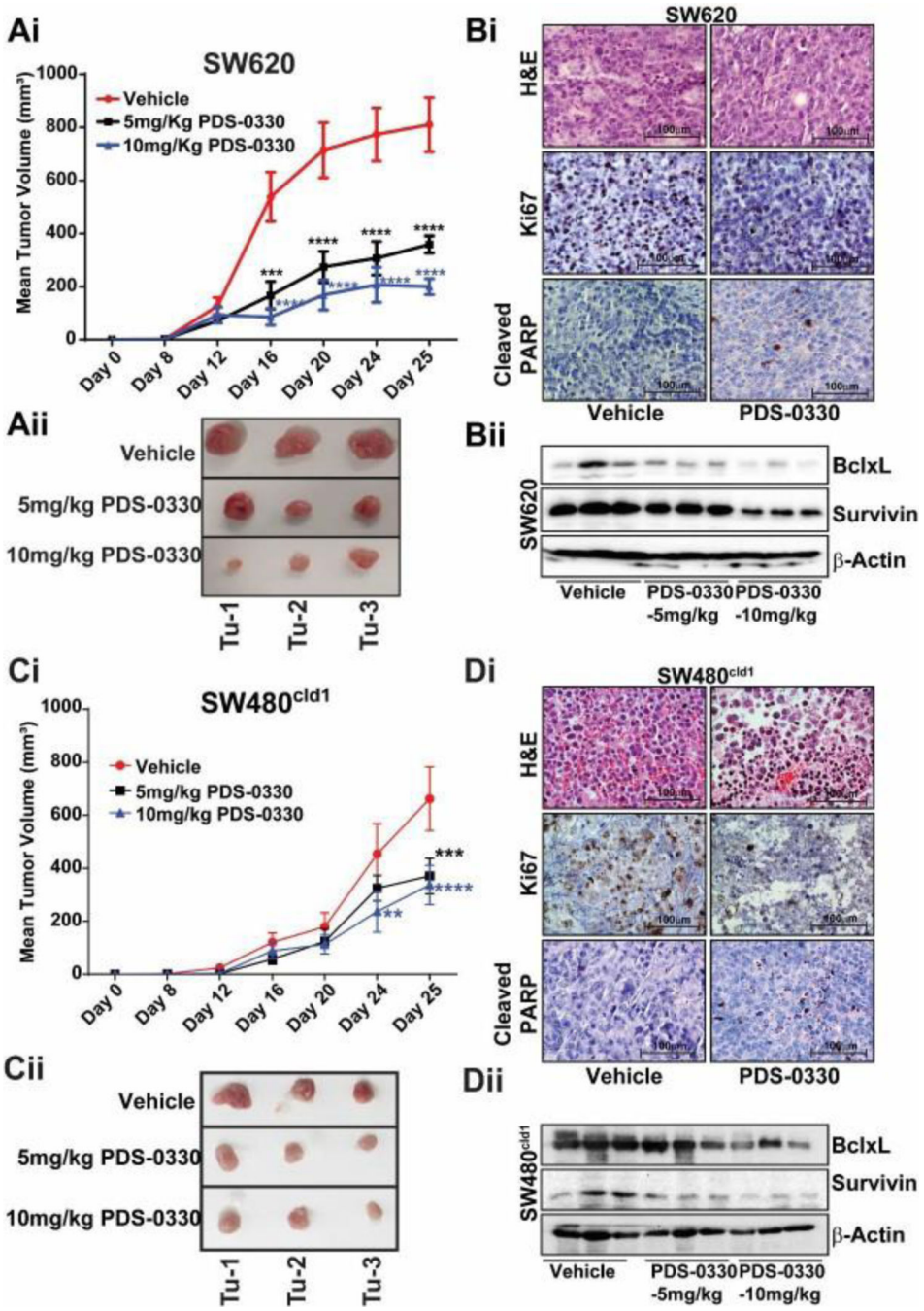

Figure 9. The anti-tumorigenic potential of PDS-0330 *in-vivo*.

(Ai & Ci) Tumor volume was measured using calipers over time (n = 5 mice per group). The formation of flank xenograft tumors in claudin-1 overexpressed SW620 and SW480^{cld1} cells injected nude mice was examined between vehicle and PDS- 0330 (5mg/kg and 10mg/kg) treatment (n = 5 mice per group).; (Aii & Cii) Representative images of tumors from the vehicle and PDS-0330 (5mg/kg and 10mg/kg) -treated nude mice.; (Bi & Di) H&E (scale equals 100 μm) and Immunohistochemical analysis (scale equals 100 μm) of proliferation marker (Ki67) and apoptotic marker (cleaved PARP) were observed in respective tumor

sections. (Bii & Dii) Apoptotic marker cleaved PARP and anti-apoptotic markers BclxL, and survivin were observed in vehicle and PDS-0330 (5mg/kg and 10mg/kg) treated SW620 and SW480^{cld1} cells xenograft tumor lysates by immunoblotting. Results analyzed by 2way ANOVA. For graphs, data represent mean ± SD; *, $P < 0.05$; **, $P < 0.01$; ***, $P < 0.001$ & ****, $P < 0.0001$.

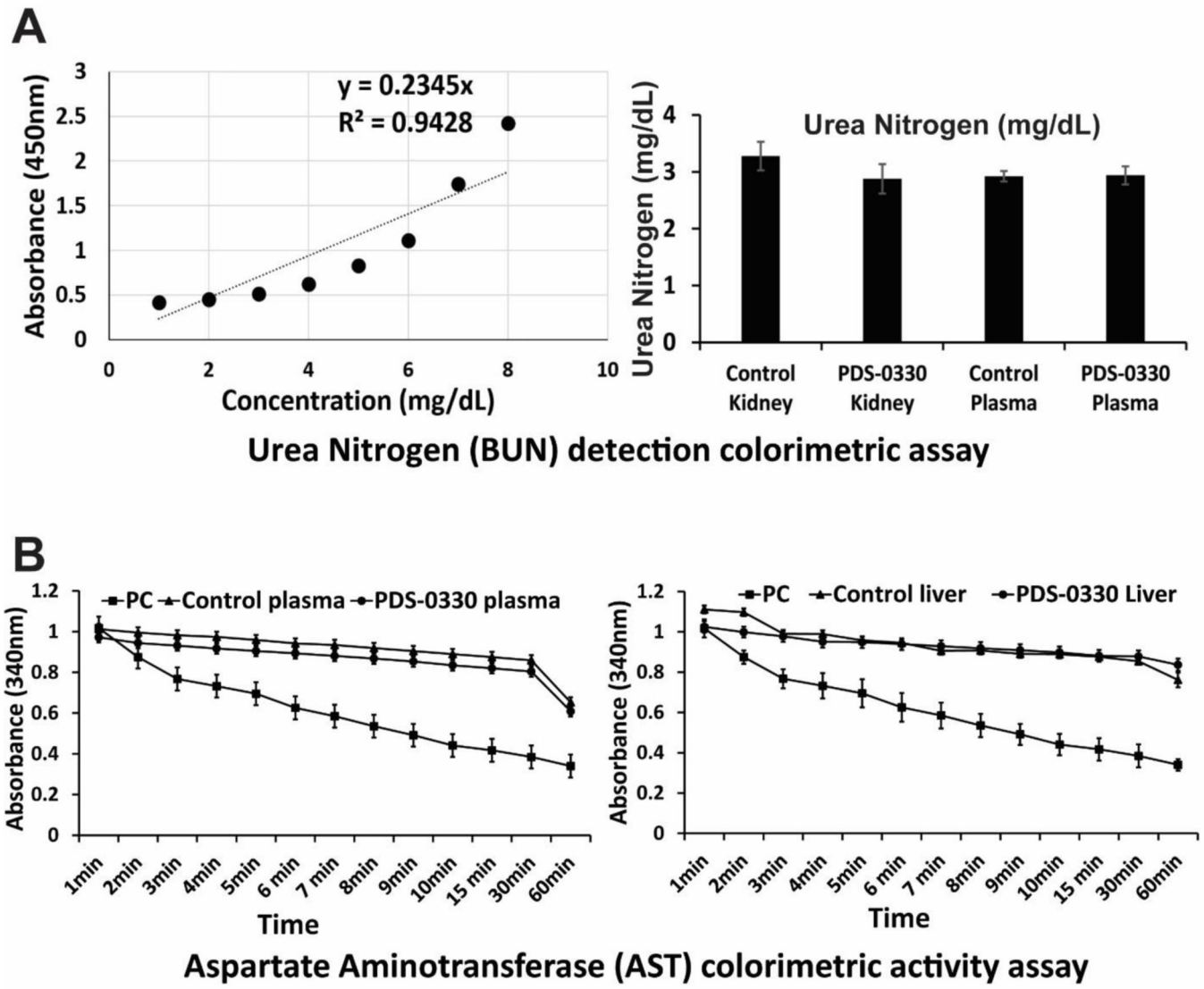

Figure 10. PDS-0330 has no cytotoxic effect in mice as measured by blood urea nitrogen (BUN) and aspartate aminotransferase (AST) levels.

(A) BUN level was measured in kidney tissue and plasma of vehicle and treated mice. (B) After sacrificing the mice at day 25, the AST activity was measured in plasma and liver homogenate of control and treated mice. The AST activity has been observed up to 60 min at regular time interval according to the standard protocol. Data are expressed as means ± SEM (n=5 mice/ group).

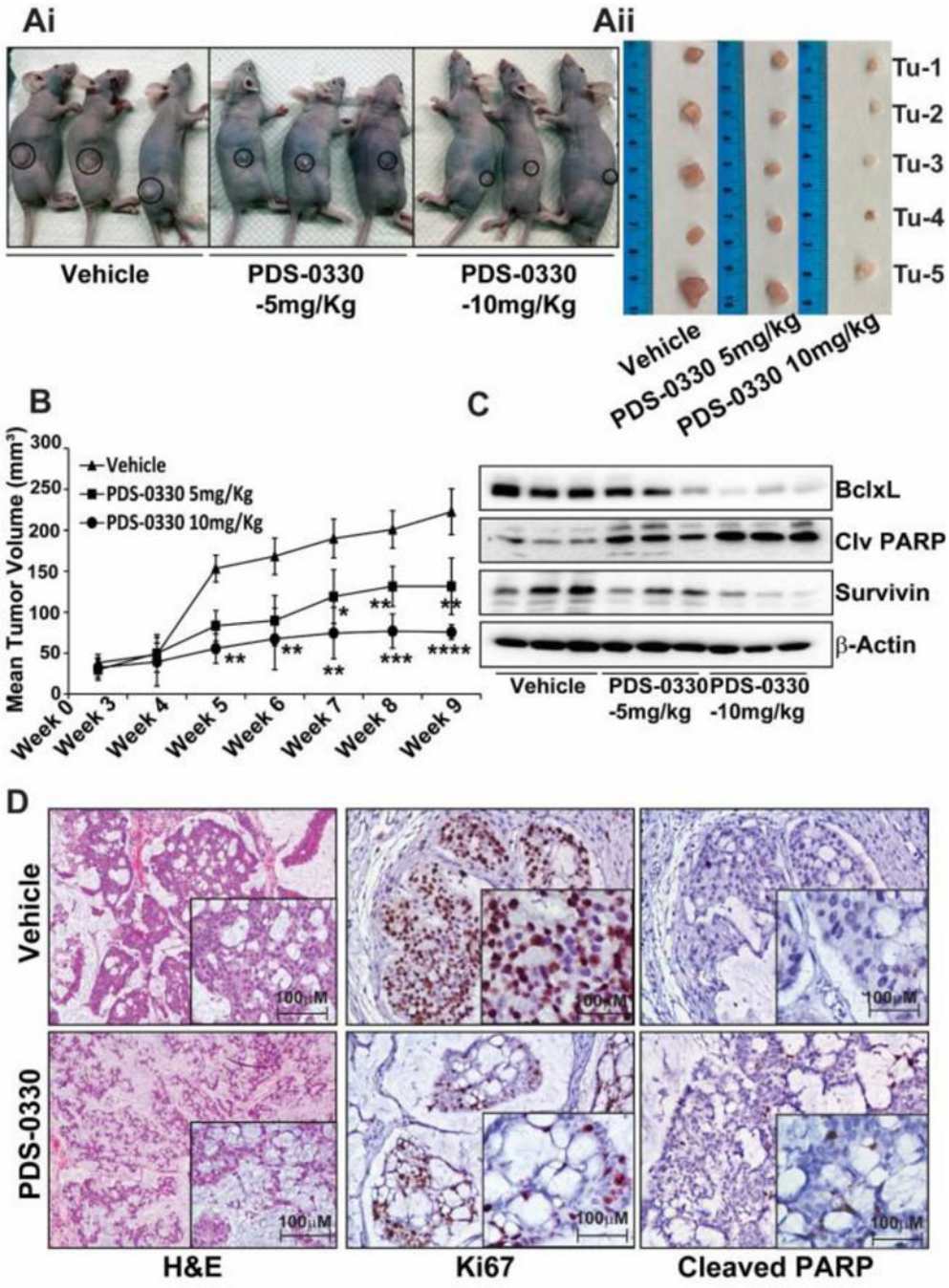

Figure 11. PDS-0330 inhibits tumor formation of claudin-1 overexpressed patient-derived xenograft nude mice.

(Ai) After implanting a claudin-1 overexpressed PDX tumor, the development of flank xenograft tumors (n = 5 mice per group) was compared to vehicle and PDS-0330 (5mg/kg and 10mg/kg) treatment.; (Aii) Representative images of tumors from the vehicle and PDS-0330 (5mg/kg and 10mg/kg) -treated nude mice.; (B) Tumor volume was tracked over time using calipers (n = 5 mice per group). (C) Apoptotic markers BclxL, cleaved PARP, and survivin were observed in the vehicle, and PDS-0330 (5mg/kg and 10mg/kg) treated PDX tumor lysates by immunoblotting.; (D) H&E (scale equals 100 μm) and

Immunohistochemical analysis (scale equals 100 μm) of proliferation marker (Ki67) and apoptotic marker (cleaved PARP) were observed in PDX tumor sections. Results analyzed by 2way ANOVA. For graphs, data represent mean ± SD; *, $P < 0.05$; **, $P < 0.01$; ***, $P < 0.001$ & ****, $P < 0.0001$.

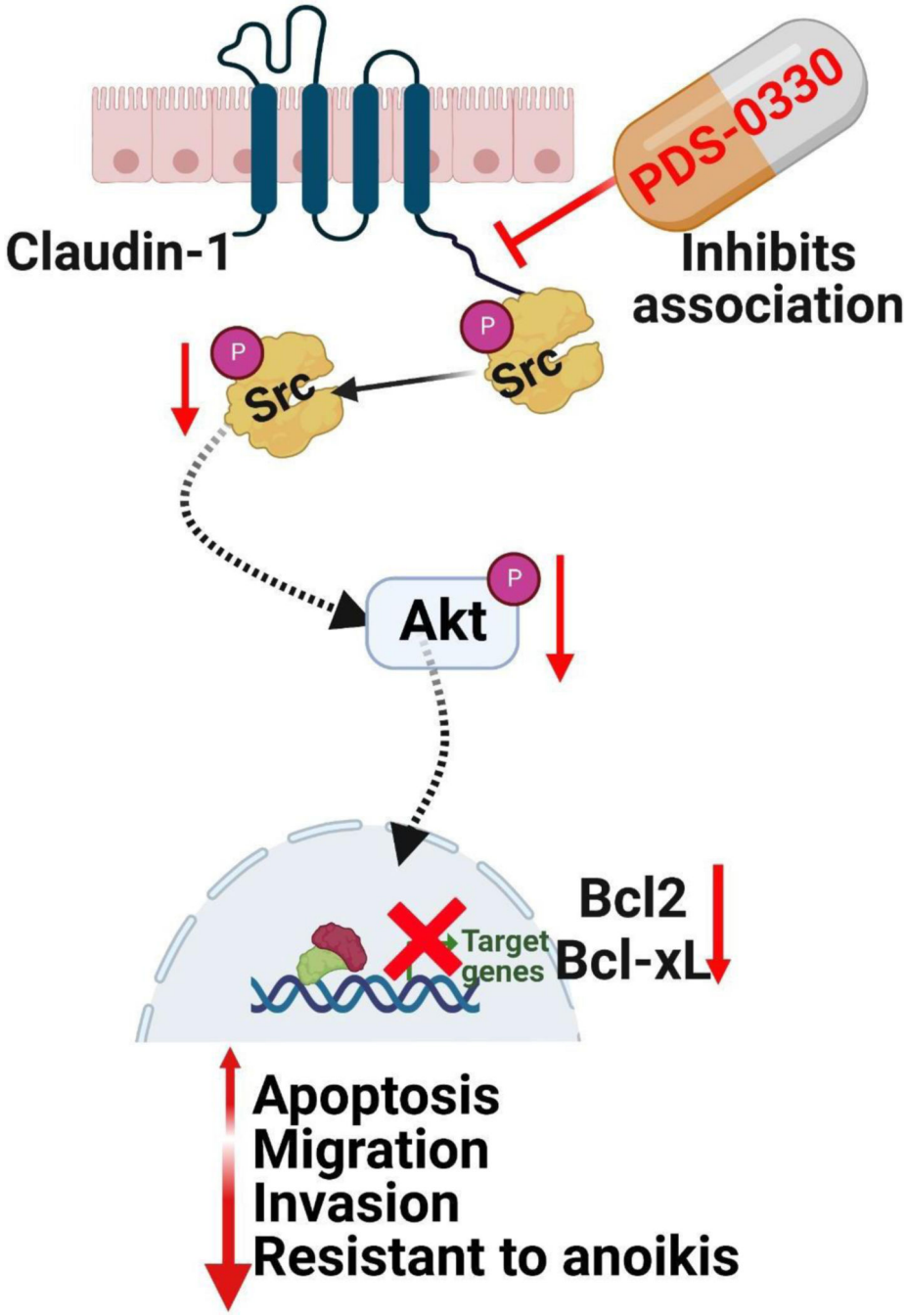

Figure 12. Graphical Abstract.

PDS-0330, a claudin-1 inhibitor, impairs the interaction between claudin1 and pSrc/Src and alters survival signaling pathways, which prevents the progression of colorectal cancer.

Table 1.

Pharmacokinetic parameters of I-6 after 1mg/kg Intra venous administration of I-6 (mean ± SD, n#5).

S.No	Parameters	Estimates (mean ± SD)
1.	C_0 (ng / ml)	798.3 ± 277.2
2.	$t_{1/2}$ (h)	7.0 ± 1.6
3.	$AUC_{0-\infty}$(h*ng / mL)	1207.1 ± 35.6
4.	$AUC_{0\text{-last}}$ (h*ng / mL)	1142.0 ± 59.6
5.	V_d (L / kg)	8.4 ± 2.1
6.	Cl (L / h/ kg)	0.8 ± 0.0
7.	MRT (h)	5.6 ± 1.2
8.	Vss (L/kg)	4.7 ± 1.1

Abbreviation: C_0: concentration at time zero, AUC: area under the curve from 0 to ∞ and last hr, Vd: volume of distribution, Cl: clearance, $t_{1/2}$: terminal half-life, MRT: mean resistance time, Vss: volume of distribution at steady state.

Table 2.

Non-compartmental Pharmacokinetic parameters of PDS-0330 after 5mg/kg post oral and 5mg/kg IP administration of PDS-0330 (mean ± SD, n=5).

Parameters (Unit)	**PO (5mg/kg)**		**IP (5mg/kg)**	
	Mean	**SD**	**Mean**	**SD**
Cmax (ng/mL)	30.8	18.3	59.3	13.8
$T_{1/2}$ (h)	14.5	9.8	5.5	1.6
T_{max}(h)	0.4	0.3	2.8	1.1
AUC_t (h*ng/mL)	53.4	14.0	422.0	206.8
$AUC_{0-\infty}$(h*ng/mL)	86.0	38.0	442.0	201.5
V_d/F (L/kg)	1095.4	409.6	126.5	105.4
Cl/F (L/h/kg)	71.5	39.8	14.7	10.0

Abbreviation: C_0: concentration at time zero, AUC: area under the curve from 0 to ∞ and last hr, Vd: volume of distribution, Cl: clearance, $t_{1/2}$: terminal half-life.

Table 3.

Tissue concentrations of PDS-0330 following oral (5mg/kg) or intraperitoneal (IP) (5mg/kg) administration (mean ± SD, n=5).

		PO (5mg/kg)		IP (5mg/kg)	
	Time	**Mean Conc. (ng/gm)**	**SD**	**Mean Conc. (ng/gm)**	**SD**
Liver	2	17.0	8.0	277.0	193.5
	8	5.8	4.8	807.1	711.8
	24	10.5	2.7	407.4	402.1
Lungs	2	5.0	3.1	337.8	236.2
	8	472.9	708.0	76.9	74.4
	24	519.0	640.7	93.7	81.0